COURSE TEXTBOOK

Department of Physics and Engineering
ITMO University

# EXPERIMENTAL METHODS OF NANOPHOTONICS

Sergey Makarov
Grigorii Verkhogliadov
Tatiana Liashenko
Ekaterina Tiguntseva
Pavel Tonkaev

Saint Petersburg
2020

# CONTENTS

# Chapter 1

# Lasers in nanoscience

## 1.1 History of Lasers

History of Light Amplification by Stimulated Emission of Radiation or LASER started 100 years ago in 1917 when Einstein proposed stimulated emission. Only 11 years later Ladenburg confirmed stimulated emission. The next important step in laser invention was made in 1940 when population inversion was discovered.

The first laser was invented in 1960 by Theodore Maiman. It consisted of three main parts: a ruby active medium, two mirrors, which form an optical cavity, and a flash tube pump. Ruby laser produces light in a visible range of a spectrum, in red colour (694 nm), with a linewidth of 0.53 nm and PCE about 1-2% (Fig. 1.1).

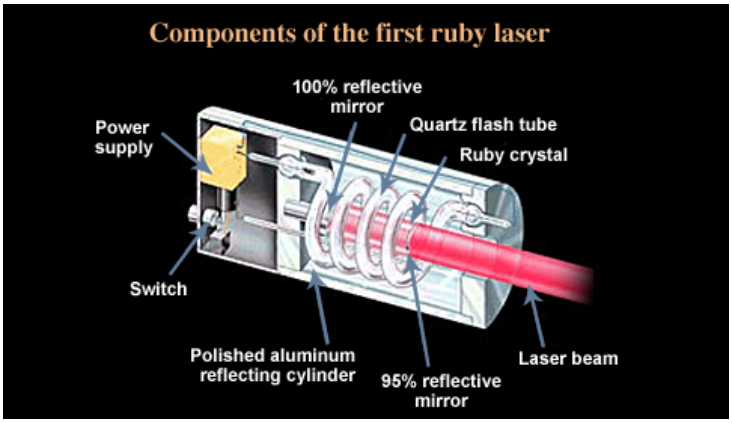


Figure 1.1: Structure of ruby laser

In 1970 Z.I. Alferov invented the first semiconductor laser or laser diode. In such kind of lasers, the laser-active medium is a pn-junction and both edges of the active layer have a mirror-like surface (Fig. 1.2). Instead of optical pumping like in a ruby laser in semiconductor laser‘s active medium excited by electric current.

Both ordinary light and laser light are electromagnetic waves, but laser light has three main advantages over ordinary light. Ordinary light is divergent and incoherent whereas laser light is highly directional and coherent. Directionality is very important for focusing and telecommunication. Ordinary light is a mixture of electromagnetic waves having different wavelengths. Laser light is monochromatic, which is very important for spectroscopy, there one wavelength and frequency is vital. Also, high monochromatic of laser light allows reducing chromatic aberration.

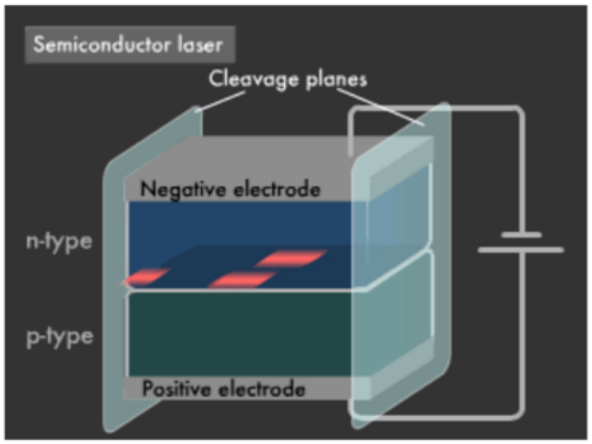


Figure 1.2: Structure of laser diode

## 1.2 Laser Applications

Due to all significant properties of lasers, it has a great number of applications in different fields of science, industrial applications, medicine and others. Laser processing can be classified into two groups: conventional laser processing and laser chemical processing. Conventional laser processing takes place without any changes in the overall chemical composition of the material. Chemical laser processing is characterized by an overall change in the chemical composition of the material or the activation of a chemical reaction.

Mechanisms of a laser beam and matter interaction depend on laser parameters and physical and chemical properties of matter. Laser light can excite free electrons in metal or vibration in an insulator. In general, this excitation energy dissipated into heat, as a consequence, a laser beam can be considered as a heat source. Figure 1.3 shows two regimes of laser-material interactions employed in conventional laser processing below and above the vaporization threshold. Regime above the vaporization threshold is characterized by plasma formation and liquid-phase expulsion [1].

Due to these properties of lasers, there are a lot of applications such as abrasive laser machining: drilling, scribing, cutting, trimming, and shaping. Material is removed as a

plasma, liquid or vapour as it is shown in Fig. 1.3 (b). With laser welding and bonding, the material is only melted. Besides laser-induced annealing, transformation hardening, glazing, recrystallization exists. All these applications use a laser with different intensity ranges.

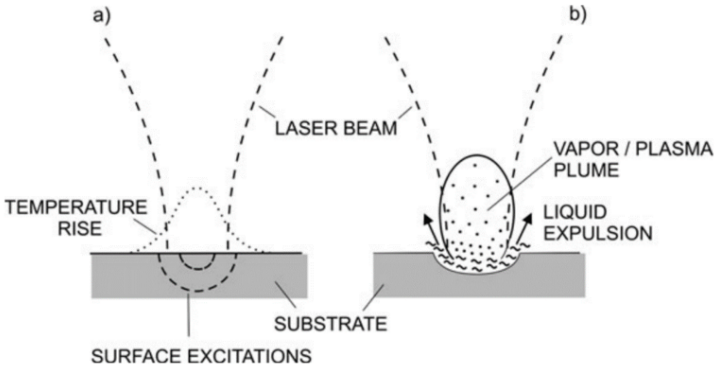


Figure 1.3: Two regimes of lasermaterial interactions. (a) below vaporization threshold and (b) above vaporization threshold [1]

Besides laser-induced thermal processes, there are non-thermal or photochemical laser processing is existed. Laser radiation can excite some molecular, which can initiate some chemical reaction or speed it up (Fig. 1.4) [1].

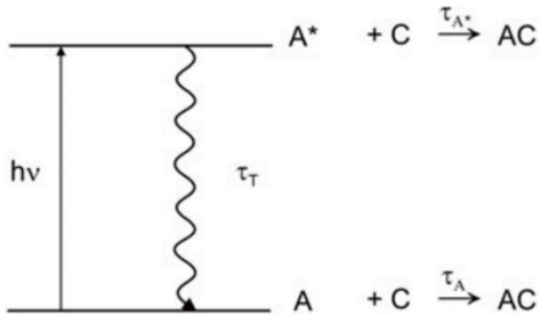


Figure 1.4: A simple model for the competition between a thermal and a photochemical reaction

.

Lasers play an important role in microscale application, for example, CD disk recording and reading. Laser diode interacts with phase-change material and due to surface heating change the optical properties of a material (Fig. 1.5). This allows writing some information in binary code on that surface. Due to differences in a reflection of irradiated and non-irradiated areas of the phase-change material information can be read from the disk.

The main challenge is to develop laser technology with the purpose to decrease the sizes of elements. The short-wave laser (about 10 nm), complicated focusing system and

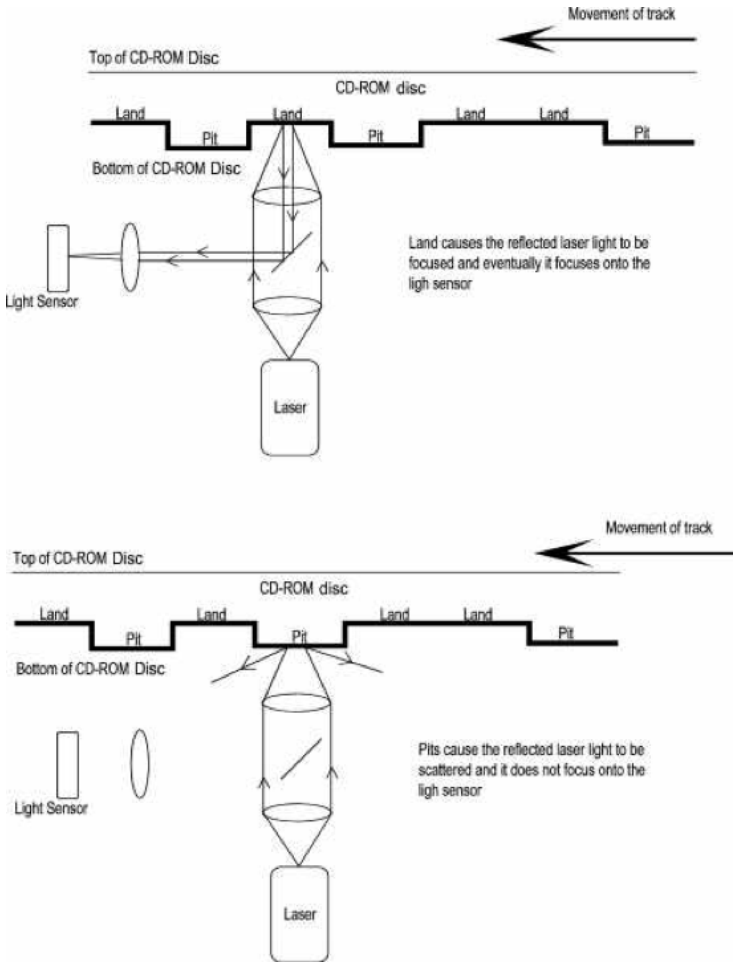


Figure 1.5: Laser recording and reading of CD disk [1]

.

new technological approaches are used for creating transistors with size of the order of 5 nm. Fig. 1.6 shows a scheme of extreme ultraviolet lithography with $CO_2$ laser and Sn plasma source with wavelength 13,5 nm.

Gas etching after the resist development allows forming small structures which are shown in Fig. 1.7.

In addition, metal surfaces have been modified and colourized with a femtosecond laser pulse and carbon dioxide lasers. Plasmon colours (structural colours that emerge from resonant interactions between light and metallic nanostructures) depends on its shape. So, laser-induced heat can change the morphology of plasmonic nanostructures due to quickly annealing as it is shown in Fig. 1.8 [2].

Direct local ablative reshaping of Au film by using irradiation of tightly focused femtosecond laser pulses. Laser pulse locally melts microscale area on the metal film which detaches from the underlying substrate and form cupola. Size of this cupola can be controlled by the energy of the pulse. Depends on size, the cupola can resonantly scatter

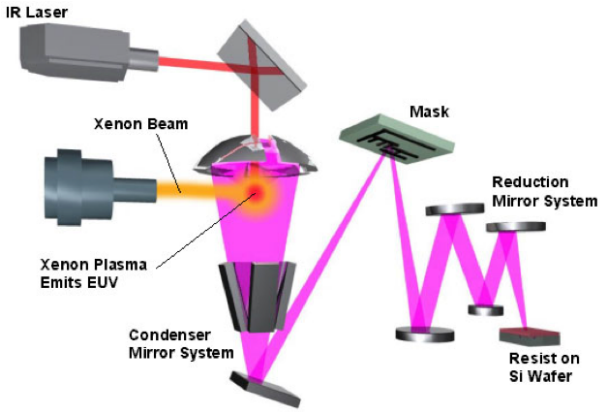


Figure 1.6: Scheme of extreme ultraviolet lithography

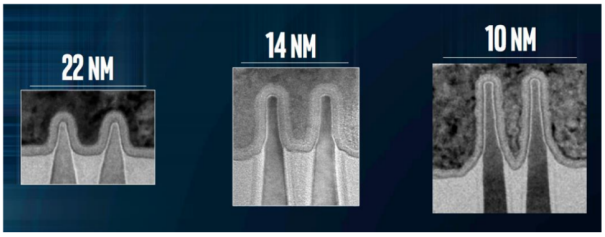


Figure 1.7: Examples of structures obtained by the extreme ultraviolet lithography

optical radiation reproducing different pure colours from green to red (Fig. 1.9 [3]).

Lasers can be applied to create 3D photonic crystals with a resolution better than 100 nm. That resolution can be achieved due to two-photon polymerization, which allows concentrating absorption in a very small area of photopolymer. Fig. 1.10 shows the difference in absorption area initiated by ultraviolet and infrared light.

Periodic order in photon crystals can provide prevention of light propagation in a certain direction or the formation of the omnidirectional complete photonic bandgap over a specic energy range. Figure 1.11 shows structures, which was created by two-photon polymerization technique and two methods for their fabrication. To create such structures femtosecond pulses centred at around 780 nm wavelength and at a repetition frequency of 80 MHz were used. 50-fs TiF-100F laser emitter was used as a source [4].

Furthermore, a laser can be used for fabrications another laser. For example, for fabrication protein-based 3D whispering gallery mode microlasers with stimulus responsiveness [5]. Laser with 150nm scanning step, 2528mW laser power and exposure time on a single point - 1000s can create 2.5-m designed thickness of laser microdisks, which are shown in Fig. 1.12.

Femtosecond lasers can form microlasers represent MAPbBrxIy microdisks with 760 nm thickness and diameters ranging from 2 to 9 $\mu$m on perovskite film, which is shown in Fig. 1.13. The diameter of microdisks is controlled by the intensity of the laser beam. That method allows fabricating single-mode perovskite microlasers, which can work at

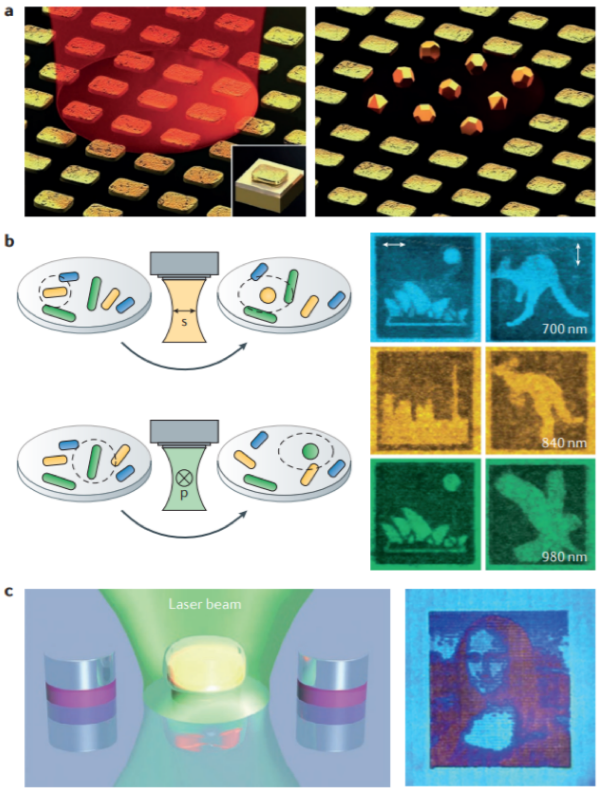


Figure 1.8: (a) Patterning and storing information in layered structures (b) or morphology changes at the single-resonator level (c)

room temperature in a spectral range from 550 to 800 nm [6].

Laser printing of silicon nanoparticles is one of the most effective way for its fabrication. Our fabrication techniques such as chemical methods, plasma synthesis, and laser ablation in air or liquids (Fig. 1.14) can produce silicon nanoparticles with different sizes, but without size control and precise deposition. Lithographic methods are more complicated and do not allow to fabricate spherical nanoparticles. One of the most effective way to synthesize silicon nanoparticles of a certain size is laser printing. In this method, silicon-on-isolator (SOI) was used as a target to transfer spherical Si nanoparticles from 50 nm crystalline Si layer onto the transparent glass receiver substrate with the femtosecond laser as a source of laser pulses at 800nm wavelength with an energy of a pulse up to 3 mJ. Size of nanoparticles is controlling by the energy of a pulse.

During laser irradiation of the SOI wafer by a laser pulse, absorption in the top Si layer leads to fast local heating and melting of that layer. If the energy of a pulse enough, silicon layer melts completely, forming a droplet induced by the surface tension. That spherical droplet has an upward-directed momentum, which drives it to the receiver substrate, where the liquid material solidifies (Fig. 1.15) [7].

One more important laser application for optoelectronics is scribing (Fig. 1.16) which allows removing one thin layer in a multilayer system without affecting on other layers.

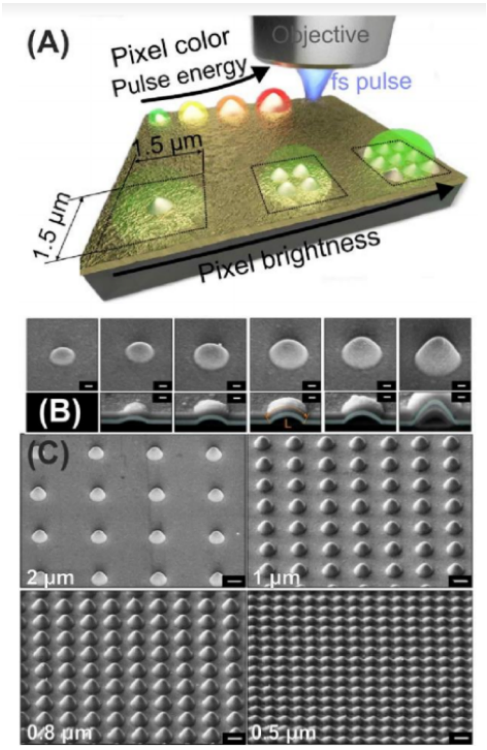


Figure 1.9: Plasmonic coloration via direct local ablative reshaping of a gold film

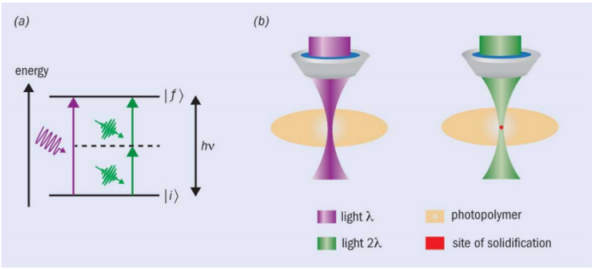


Figure 1.10: Absorption in photopolymer initiated by ultraviolet and infrared light

Laser scribing allows separating modules via cutting small pieces of a structure. Scribing has application in many semiconductor technologies, which are characterized by relatively small wafers having narrow die-separation streets. LED wafers are expensive, so wafer real estate is valuable. Ultraviolet lasers provide narrow and clean cuts, and as a result, a better die count per wafer as well as higher yields, due to fewer damaged die than with common scribing methods.

Moreover, lasers can be applied for producing so-called black silicon (Fig. 1.17). Such material is a surface modification of silicon with low reflectivity and high absorption of visible and infrared light. Silicon surface irradiated with femtosecond laser pulses in the presence of sulfur hexafluoride gas or in vacuum. As a result, silicon surface develops

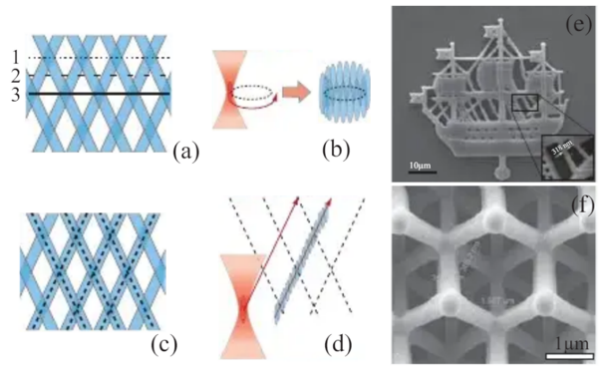


Figure 1.11: Two methods for fabrication 3D structures by the two-photon polymerization technology: raster scanning (a,b) and vector scanning (c,d); structures fabricated using raster (e) and vector (f) scanning approach

.

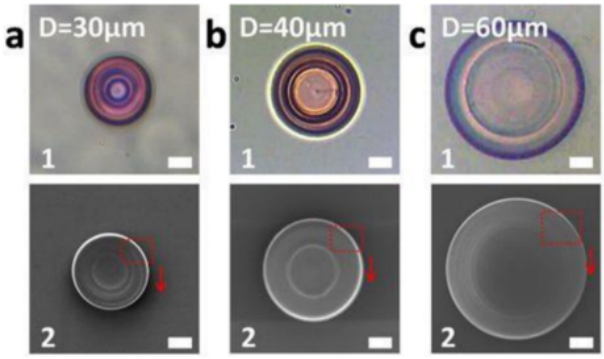


Figure 1.12: The protein-based 3D WGM microdisk with diameter of 30m (a), 40m (b) and 60m (c). 1, top-view OM image; 2, top-view SEM image

.

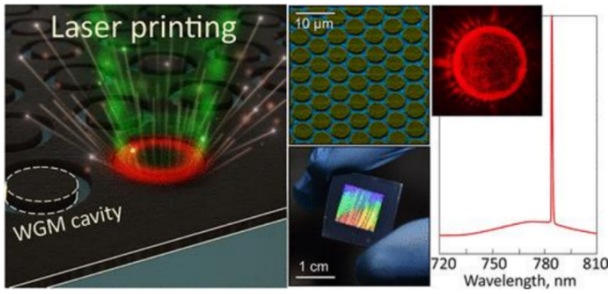


Figure 1.13: Single-mode perovskite lasing microdisks

.

structure of micrometer-sized cones. That material has absorption that extends to the infrared range, below the band gap of silicon, including wavelengths for which ordinary

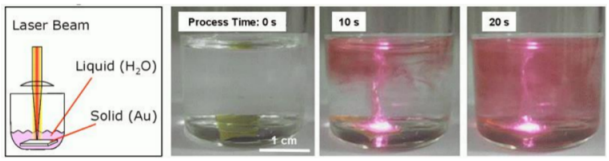


Figure 1.14: Laser ablation in liquids

.

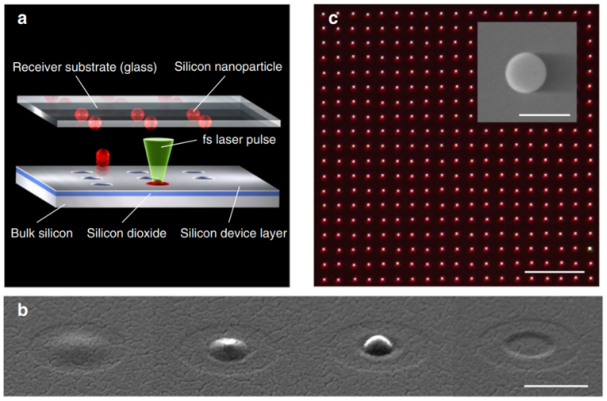


Figure 1.15: Laser-printing process of Si nanoparticles. (a) Schematic illustration of femtosecond laser printing of nanoparticles. (b) SEM images of the target before and after nanoparticle-ejection process from the SOI substrate. From left to right, the laser pulse energy is gradually increased. (c) Array of several hundreds of amorphous Si nanoparticles fabricated by this method

.

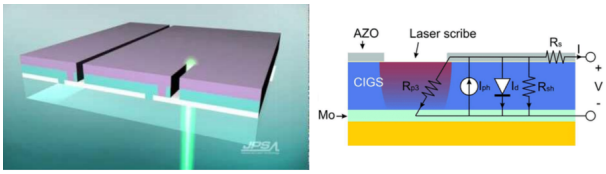


Figure 1.16: Laser scribing

.

silicon is transparent.

Laser surface modification allows making super-hydrophobic coating, which is extremely difficult to wet. The contact angles of a water droplet on a super-hydrophobic material exceed 150 (Fig.1.18). Such coating is extremely important for photovoltaic because of improved absorption and protection from rain droplet with some dirties.

Laser plays an important role in medicine. A laser is applied for warts and tattoos removal due to heating and some photochemical reactions. Femtosecond lasers are used in eye surgery due to reshaping the front surface of the eye for better focusing. It can correct short-sightedness, long-sightedness and astigmatism. The UV light is absorbed

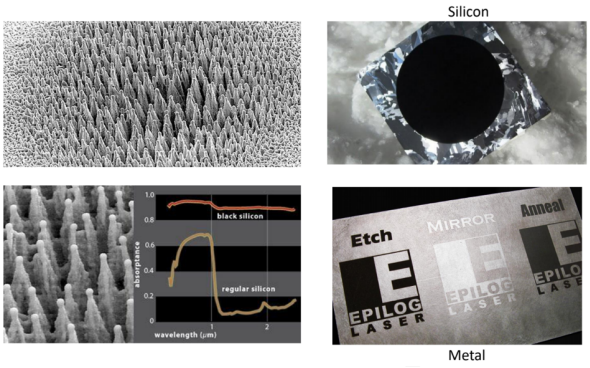


Figure 1.17: Black silicon. Surface structure and absorption

.

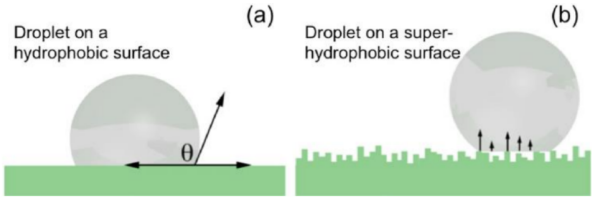


Figure 1.18: Hydrophobic (a) and super-hydrophobic (b) surface

.

in a very thin layer of tissue, decomposing that tissue into a vapor of small molecules, which fly away from the surface in a tiny plume. This happens so fast that nearly all of the deposited heat energy is carried away in the plume, leaving too little energy behind to damage the adjacent tissue.

One of the most perspective laser application in medicine is micro- and nano-laser surgery, which can provide the removing of tumour cells (Fig. 1.19). Firstly, we synthesize nanoparticles which absorb radiation at a specific wavelength and cover it with some additional organic. Those nanoparticles covered by organic form bind only with a tumour cell. Laser irradiation is with intensity less of a burning cell, but with an intensity which strongly heats nanoparticles and destroys tumour cell.

The miniaturization and integration of photonic components has improved systems and opened up a wide variety of new application areas, somewhat in analogy to developments in electronics. Applications of ever-smaller lasers include on-chip optical communications and data-processing, which may allow data rates beyond what is feasible in the realm of electronics. Progress in laser miniaturization over the past few decades is summarized in Fig. 1.20, with the images scaled in size to the lasing wavelength of the laser shown in each panel. It seems to take 10-20 years from the initial proof-of-concept of lasing, often performed at low temperature, until devices useful for applications are obtained. Practical devices typically require continuous wave (CW) operation at room temperature, ideally with direct electrical pumping, a reasonably long lifetime and par-

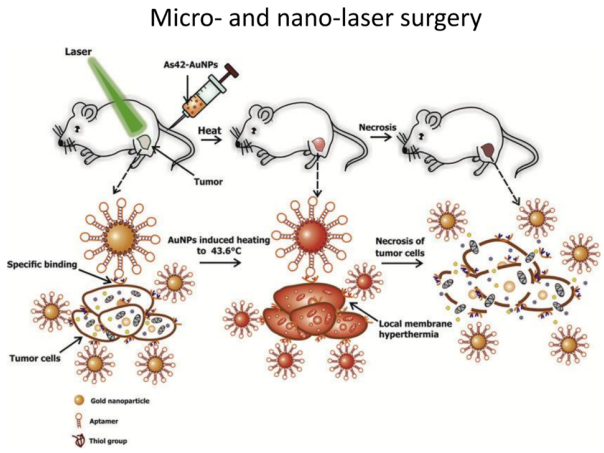


Figure 1.19: Micro- and nano-laser surgery for tumor cells removal

.

ticular characteristics that established types of lasers cannot offer.[9]

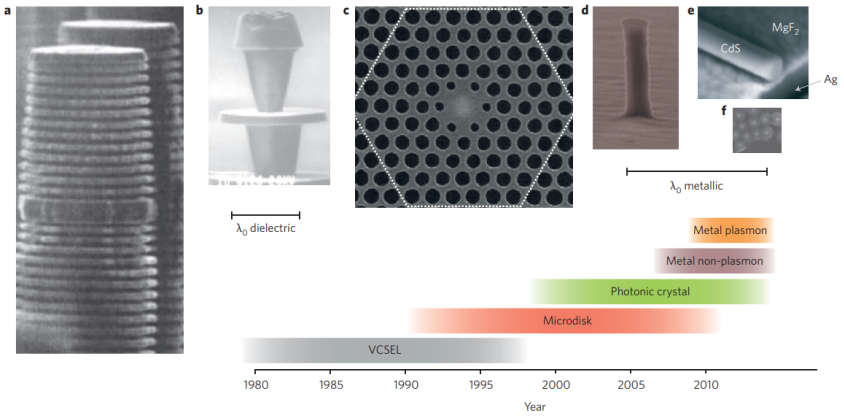


Figure 1.20: r. a) VCSEL b) Microdisk laser c) Photonic crystal laser d) Metallic non-plasmon mode laser e) Metallic propagating plasmon mode laser f) Localized plasmon mode laser. The free-space wavelength scale of the metal-cavity based lasers (d-f) is twice that of the dielectric lasers (a-c)[9]

.

# References

1. Buerle D. Laser processing and chemistry. Springer Science Business Media, 2013.

2. Kristensen A. et al. Plasmonic colour generation //Nature Reviews Materials. 2017. . 2. . 1. . 16088.

3. Wang X. et al. Single-step laser plasmonic coloration of metal films //ACS applied materials interfaces. 2017. . 10. . 1. . 1422-1427.

4. Rybin M. et al. Band structure of photonic crystals fabricated by two-photon polymerization //Crystals. 2015. . 5. . 1. . 61-73.

5. Sun Y. L. et al. Protein-based three-dimensional whispering-gallery-mode microlasers with stimulus-responsiveness //Scientific reports. 2015. . 5. . 12852.

6. Zhizhchenko A. et al. Single-Mode Lasing from Imprinted Halide-Perovskite Microdisks //ACS nano. 2019. . 13. . 4. . 4140-4147.

7. Zywietz U. et al. Laser printing of silicon nanoparticles with resonant optical electric and magnetic responses //Nature communications. 2014. . 5. . 3402.

8. https://spie.org/news/1411-single-wavelength-hybrid-silicon-lasers?SSO=1

9. Hill M. T., Gather M. C. Advances in small lasers //Nature Photonics. 2014. . 8. . 12. . 908.

# Chapter 2

# Properties of laser emission

## 2.1 Basic principles of laser

---

For understanding the main ideas behind laser operation, terms such as induced absorption, spontaneous emission, and stimulated emission are explained below. The following terms will be describe within the scope of the two levels system of some atom or molecule with energies $E_1$ and $E_2$ ($E_1 < E_2$).

1. Induced absorption. In the case of two levels system, the photon with sufficient energy comes to the system (according the Fermis golden rule). The incident photon is absorbed by the atom in ground state $E_1$ thereby leaving the atom in the excited state $E_2$.

2. Spontaneous emission. In this case, the atom emits a photon of energy $h\nu_0 = E_2 - E_1$ in any direction. This process, which is co-called relaxation, can happen in a different period, but the system should relax to the lowest state. This process called spontaneous because no external force is applied for occurring this process.

3. Stimulated emission. As applied to this emission, the mechanism of the process is the same as in spontaneous emission, but the atom is stimulated by an external photon. In this case, the incident photon if energy $h\nu_0 = E_2 - E_1$ induces the atom to decay by emitting a photon that travels in the direction of the incident photon. For each incident photon going in the same direction. In this way, we can get, an amplified as well as unidirectional coherent beam.

Turning to the concept of the probabilities of these processes let introduce N as the number of atoms or molecules per unit volume. The quantity of N is called the population of the level. Albert Einstein proposed the rates of these processes (how many transitions happen per second) in 1916.

For the case of absorption rate we can write

$$\frac{\partial N_1}{\partial t} = N_1 B_{12} \rho(\nu). \tag{2.1}$$

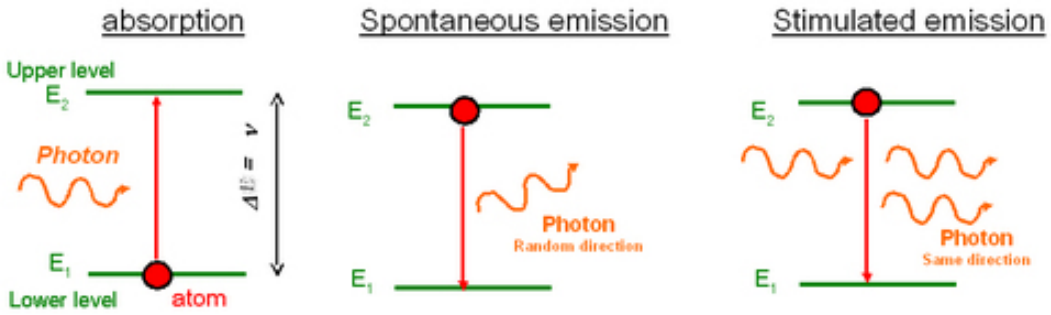


Figure 2.1: The mechanism of the interaction between an atom and a photon

For stimulation emission we can write

$$\frac{\partial N_2}{\partial t} = N_2 B_{21} \rho(\nu). \tag{2.2}$$

We can write spontaneous emission rate

$$\frac{\partial N_2}{\partial t} = N_2 A_{21} \rho(\nu). \tag{2.3}$$

where $N_1$ is the population of the lower laser level 1, $N_2$ is the population of the upper laser level 2, $\rho(\nu)$ is the energy density of the incident radiation and $N_1$ and $N_2$ are the population of states 1 and 2 respectively, $A_{21}$ is the Einstein coefficient or rate of spontaneous emission, $B_{12}$ and $B_{21}$ are the Einstein coefficients (or rate) for photon absorption and induced emission respectively

Under thermal conditions the population of two states 1 and 2, is determined by the Bolztzman distribution:

$$\frac{N_1}{N_2} = exp(\frac{-\Delta E}{kT}). \tag{2.4}$$

where $\Delta$ E is the energy difference between two states, T is the temperature, and k is the Boltzmanns constant. $N_2$ is always less than $N_1$ [1].

Lets consider first the Buger-Lambert-Beer law which describe the exponential decrease of the monochromatic light intensity passes through absorption medium (Fig 2.2).

$$I = I_0 exp^{-\alpha l}. \tag{2.5}$$

$I$ is an intensity of emergent beam, $I_0$ is an intensity of incident beam, $c$ is a concentration of absorption solution, $\alpha$ is an absorption coefficient and $l$ is the length of absorption medium.

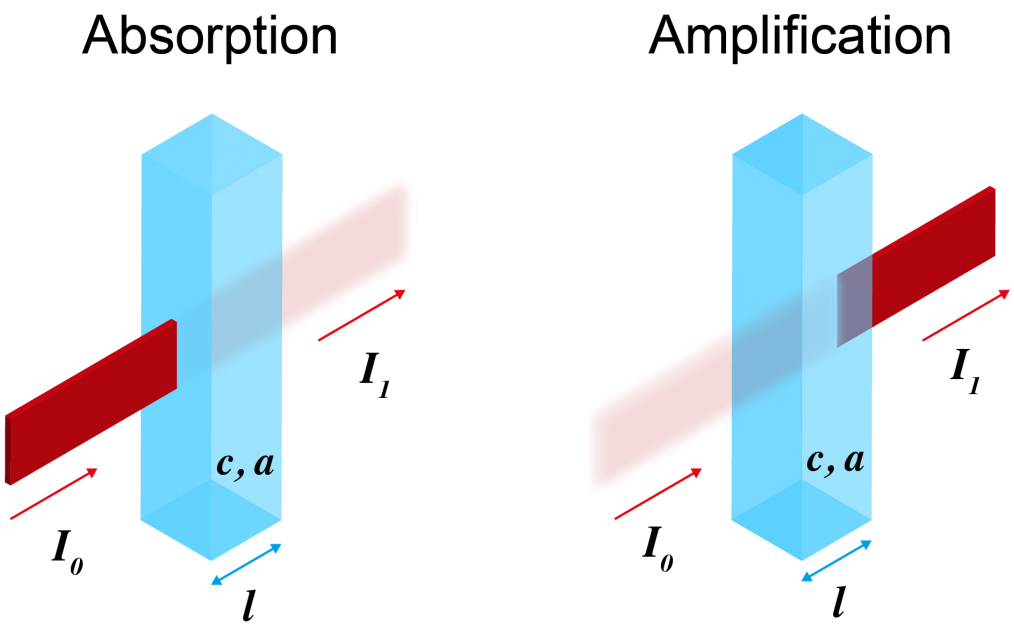


Figure 2.2: The schematic diagrams of absorption and amplification processes.

In case of laser, the strong stimulated emission is required and as a consequence, a lot of electrons in the upper state $N_2$ which is called population inversion ($N_2 > N_1$). Amplification is governed by the gain coefficient $g$ (Fig. 2.2).

$$I = I_0 exp^{+gl}. \tag{2.6}$$

Consider the change in intensity of a beam as it passes through a thin slice of material, as illustrated in figure 2.3:

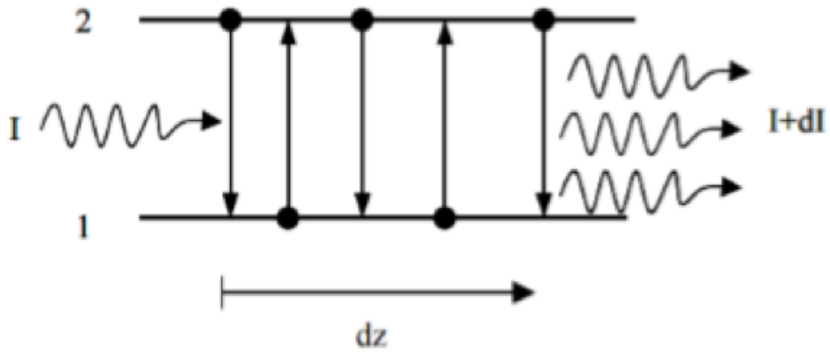


Figure 2.3: The change of a beam intensity passes through a slice of a material

$$\partial I = (N_2 B_{21} - N_1 B_{12}) \frac{I}{c} h\nu \partial z. \tag{2.7}$$

Difference between stimulated emission and negative process for amplification, dz is a direction of propagation. The spontaneous emission has been neglected. Since $B_{21}$=$B_{12}$

$$\frac{\partial I}{\partial z} = (N_2 - N_1) B_{21} \frac{I}{c} h\nu. \tag{2.8}$$

Solving the differential equation we get the similar law as Beer law, but for amplification:

$$I_z = I_0 exp^{\gamma x}. \tag{2.9}$$

Where the gain coefficient $\gamma$ is equal to g is given by

$$\gamma = (N_2 - N_1) B_{21} \frac{h\nu}{c} = (N_2 - N_1)\sigma = g. \tag{2.10}$$

where $\sigma$ ($cm^2$) is the stimulated emission cross-section. For the systems if we have separate atoms, separate ions generated light, all of them can be characterized by cross-section of stimulated emission. For $\gamma > 0$, the intensity of the light will increase as it passes through the material i.e. there will be optical gain

$$g(h\omega) = \frac{\pi e^2}{n_r c \varepsilon_0 m_0^2 \omega} |M|^2 \int_0^\infty \rho_r (f_c - f_\nu) \frac{\hbar/\pi\tau_{in}}{(E_g + E - \hbar\omega)^2 + (\hbar/(\tau_{in})^2} \partial E. \tag{2.11}$$

M is the probability

$\rho_r$ is the density of states

$\tau_{in}$ - the intraband scattering lifetime of carriers (0.1 ps),

$f_c$ and $f_\nu$ - the Fermi distribution functions for electrons and holes, respectively. $f_c$ - $f_\nu$ is an inversion [1].

As it is well known there are two types of semiconductors classified according the energy band distribution in wavenumber space:

1.Direct semiconductors (Si and Ge)

2.Indirect band gap semiconductors (GaAs, InAs and so on).

Fig. 2.4 shows the band energy diagram for direct semiconductors, where the maximum of valence band and the minimum of conduction have the same value of wavenumber (k). In this case, exiting electrons and electrons-holes recombination are direct process which required only photons. But in indirect semiconductors (Fig. 2.4 (b)), due to the difference in wavenumber value between the maximum of valence band and the minimum of conduction band, the emission process required additional change of crystal momentum (phonon). But photons cannot carry crystal momentum; therefore, the efficiency of

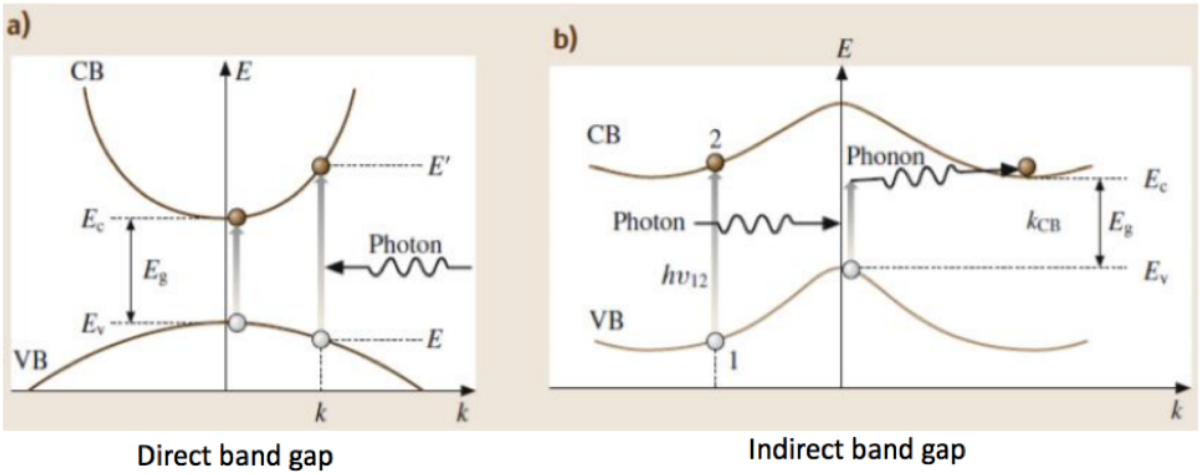


Figure 2.4: Schematic band diagrams for the emission processes in: (a) direct band gap semiconductors and (b) indirect band gap material gap semiconductors

emission of indirect band gap semiconductors is much smaller than that of direct band gap semiconductors [2].

The density of states (DOS) is the number of different states at a particular energy level that electrons are allowed to occupy, i.e. the number of electron states per unit volume per unit energy. In semiconductors, the free motion of carriers is limited to two, one, and zero spatial dimensions. When applying semiconductor statistics to systems of these dimensions, the density of states in quantum wells (2D), quantum wires (1D), and quantum dots (0D) must be known.

3-D (bulk)

$$g(E) = \frac{1}{2\pi^2}\left(\frac{2m^*}{\hbar^2}\right)^{3/2}\sqrt{E_g - E}. \tag{2.12}$$

2-D (bulk)

$$g(E) = \frac{m^*}{\pi\hbar^2}\sigma(E_g - E). \tag{2.13}$$

1-D (bulk)

$$g(E) = \frac{m^*}{\pi\hbar}\sqrt{\frac{m^*}{2(E_g - E)}}. \tag{2.14}$$

0-D (bulk)

$$g(E) = 2\delta(E_g - E). \tag{2.15}$$

The variable Stripe Length Method (VSLM) is a very popular tool to measure the optical gain which has been demonstrated by Shaklee and Leheny in 1971 [3]. In the VSLM

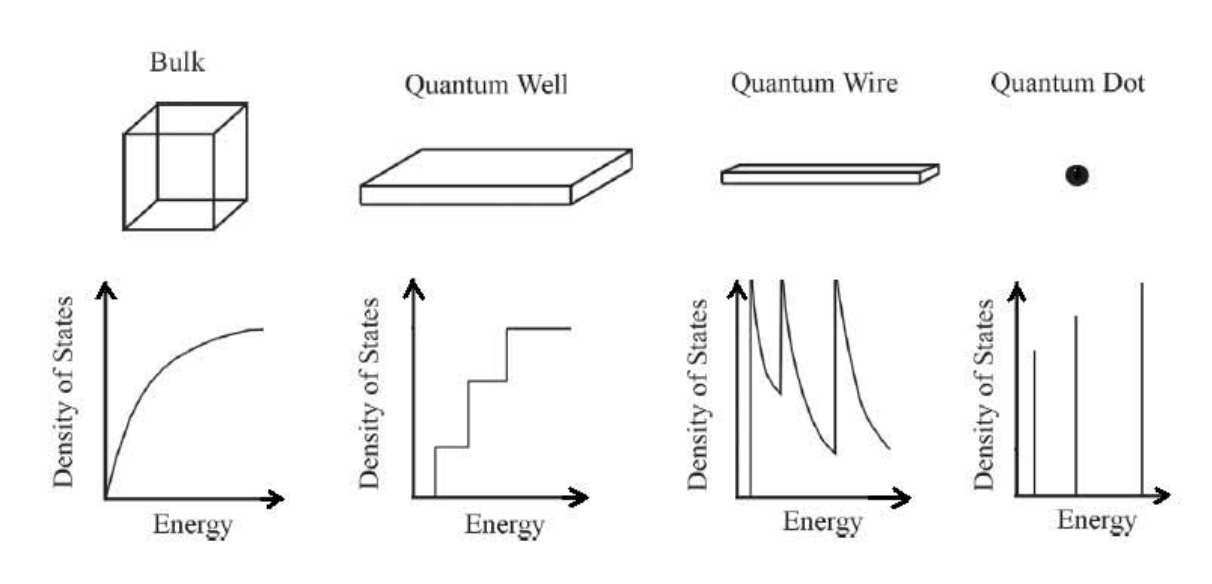


Figure 2.5: Density of states vs. energy for bulk material, quantum well, quantum wire and quantum dot

method, the sample is pumped by an intense homogeneous laser beam, which is focused by a cylindrical lens to form a narrow stripe on the sample surface (Fig. 2.6). The length z of the stripe can be varied through a movable (variable) slit. When the length of the stripe is short, the photoluminescence spectrum is broad. But, by increasing the length of the stripe, the emitted intensity increases super-linearly and the spectrum becomes narrower. The same behavior is observed by increasing the pump energy at a constant stripe length as shown in Fig. 2.7. An amplified spontaneous emission (ASE) signal $I_{ASE}$(z) is collected from the edge of the sample as a function of $z$. As a result of population inversion achieved at high pumping rates, spontaneously emitted light is amplified and an intense, and partially coherent ASE signal grows up exponentially increasing the excitation length $z$ [4].

[Dal Negro L. et al. Applicability conditions and experimental analysis of the variable stripe length method for gain measurements //Optics communications. 2004. . 229. . 1-6. . 337-348.]

The big advantage of such a widely used experimental method is that no special sample preparation is needed and transparent as well opaque samples are equally suited for gain measurements. In addition, the basic principle of the technique is extremely simple: the one-dimensional amplifier model.

For analyzing measured data let's consider an optical amplifier which represents the illuminated stripe where the width of the stripe is very small compare to the length. This one-dimensional optical amplifier has cylindrical shape with length $l$ and cross sectional area $s$. The ASE emission is assumed to be in both z-directions and the solid angle which is seen from zero position is $\sigma$ but the solid angle of the differential element $\partial z$ is $\sigma$(z) (Fig.

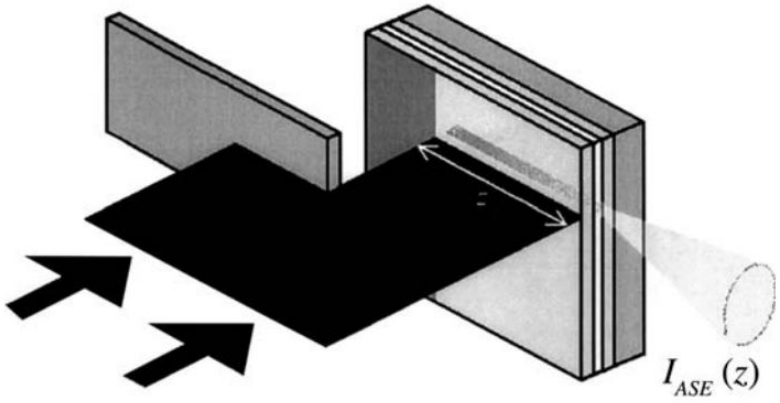


Figure 2.6: Sketch of the variable stripe length configuration. The amplified spontaneous luminescence Intensity $I_{ASE}$(z) is collected fromthe edge of the sample as a function of the excitation length z. The laser beam is focused on a thin stripe by a cylindrical lens.[4]

2.8). In low saturation regime, the intensity from the differential element $\partial z$ which emits from the facet of the amplifier consists of stimulated emission and spontaneous emission and can be written as:

$$\frac{\partial I}{\partial z} = (\Gamma g_m - \alpha)I + (S_{sp}N^* h\nu)(\frac{\Omega(z)}{4\pi}). \tag{2.16}$$

The gain and the pump intensity are assumed to be constant over the whole pumping length, and the equation above can be easily integrated. By using the boundary condition, the ASE emission can be written as:

$$I_{ASE}(z) = \frac{J_{sp}(\Omega)}{g}(e^{gz} - 1). \tag{2.17}$$

The spontaneous emission intensity emitted within the solid angle and is the net modal gain of the material, defined as $g = \Gamma g_m - \alpha$.

$$J_{sp}(\Omega) = \frac{A_{sp}N^* h\nu\Omega}{4\pi}. \tag{2.18}$$

For simplicity, we will consider $\Gamma$=1 and $\alpha$=0.

$\Gamma$ is the confinement factor for the waveguide structure, $g_m$ is the material gain, $\alpha$ is the propagation loss coefficient, $S_{sp}$ is the spontaneous emission rate, $I$ is the intensity, $N^*$ is the excited state population density and is the energy of the emitted photon, $\Omega(z)$ is the solid angle of the different element dz, $I_{ASE}$ (amplified spontaneous emission) narrowing like on previous picture, $g$ is the modal gain [4].

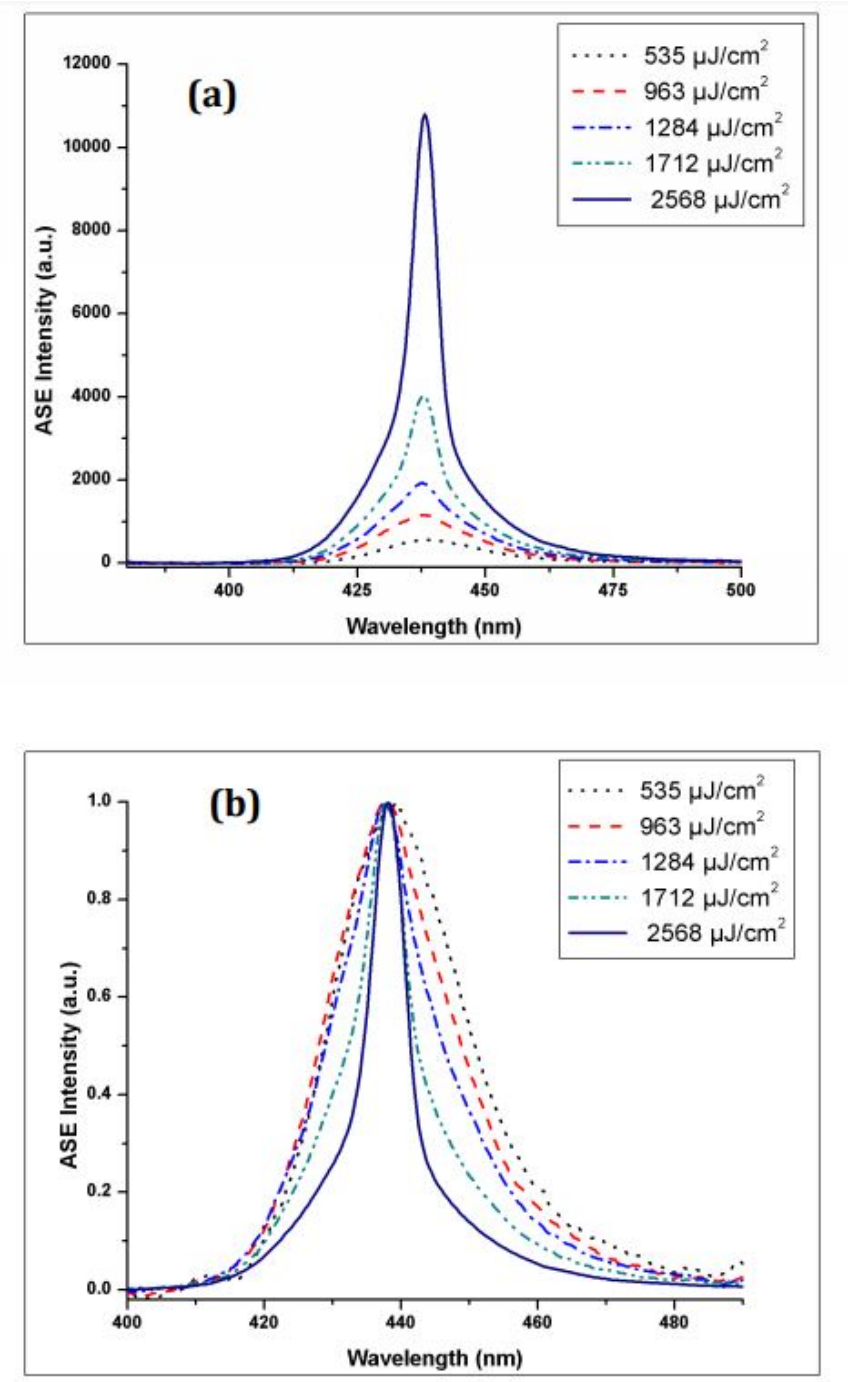


Figure 2.7: ASE Intensity vs. wavelength at different pump energies and stripe length of 3 mm from InGaN: (a) absolute intensity and (b) normalized intensity.

Some optical gain values for different semiconductor materials measured with VSLM are given in Fig. 2.9.

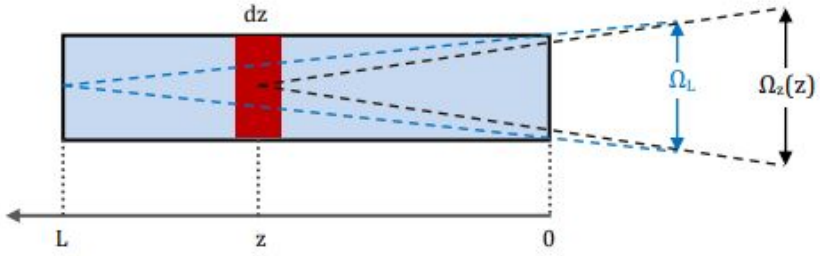


Figure 2.8: ASE along the illuminated stripe [3].

| Semiconductor material | | Optical gain for $10^7$ W/cm$^2$and 2 °K (cm$^{-1}$) | Wavelength of the peak gain (nm) |
|---|---|---|---|
| III-V | GaAs | 2000 | 820 |
| | GaP : N | 10000 | 540 |
| | GaP : Bi | 175 | 555.4 |
| | GaN | 1000 | 359 |
| II-VI | CdS | 200 | 490.5 |
| | CdSe | 1000 | 684 |
| I-VII | CuCl | 6400 | 392 |
| III-VI | GaSe | 10000 | 600 |

Figure 2.9: Optical gain measurements for different semiconductor materials [5].

What do we need to create laser?

1. Pump source: external energy
2. Active medium: amplification, coherence
3. Resonator: positive feedback, directivity

Gain and cavity

Optical gain is not sufficient to obtain laser operation, which is the oscillation of light in a resonator. For having lasing, we need to provide a good cavity. In this case, we need to consider the losses of whole cavity. We need cavity because it gives us positive feedback, to let photons go many times in the active medium and amplify signal repeatedly. For oscillation, we need:

1. Gain Losses, i.e. $\gamma \geqslant \alpha$ (where the loss coefficient, ¿0). In case, losses and gain are equal we have threshold, if less enhancements than losses decrease of energy (absorption). Losses can be roughness, some impurities and so on.

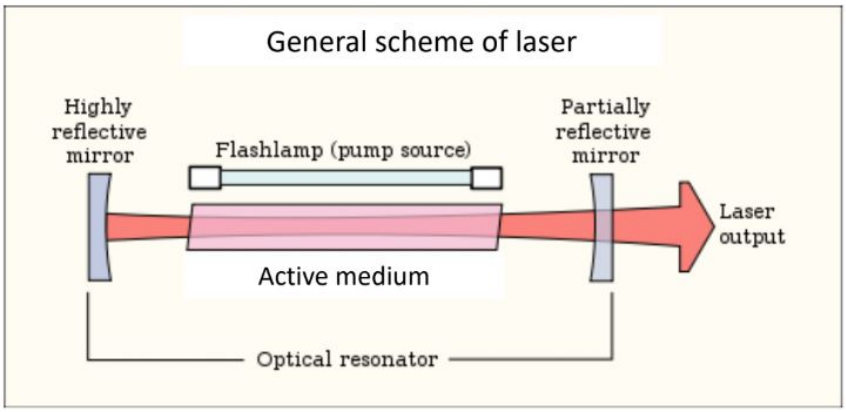


Figure 2.10: General scheme of laser.

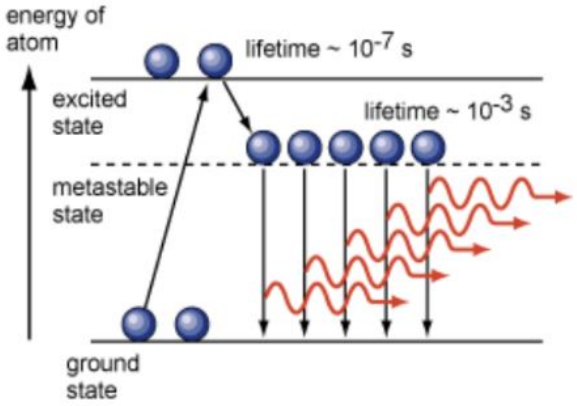


Figure 2.11: Inversion population

2. Positive feedback For $\gamma > 0$, we require N2¿N1 but for any thermal population distribution $N_2 < N_1$ We therefore need to excite or pump the material, known as the gain medium, to get $N_2 > N_1$ (typically by illuminating with another light source of by passing an electric current though the material). The condition of N=$N_2 - N_1 > 0$ is known as a population inversion.

Now the rate equation becomes

$$N_2 = -N_2 B_{21}\rho - A_{12}N_2 + N_1 B_{12}\rho + R \tag{2.19}$$

where R is the pump rate i.e. the rate of excitation to level 2.

$R_2$, $R_1$ are radii of curvature

L is length of the active medium

Evolution of spontaneously emitted photons:

Normally photons emitted from active medium and only small part of these photons which emit along the axis of the resonator start to propagate many times in this direction.

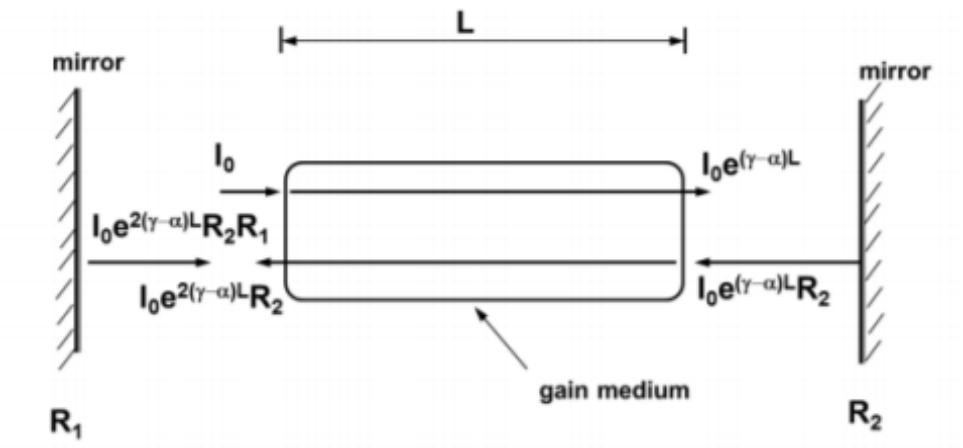


Figure 2.12: Gain and loss during a cavity round trip

After passing through the gain medium for the first time, it experiences net gain (i.e. gain exceeds the loss) and the intensity is:

$$I_0 exp[(\gamma - \alpha)L]. \tag{2.20}$$

and after subsequent reflection from the right-hand mirror it becomes:

$$I_0 exp[(\gamma - \alpha)L]R_2. \tag{2.21}$$

It then passes back through the gain medium and at this point it is

$$I_0 exp[2(\gamma - \alpha)L]R_2. \tag{2.22}$$

It is then reflected by the left-hand mirror so that when it returns to its starting position it is now:

$$I_0 exp[2(\gamma - \alpha)L]R_1R_2. \tag{2.23}$$

For steady-state operation, we require that there is no change after one round-trip i.e.

$$I_0 = I_0 exp[2(\gamma_{th} - \alpha)L]R_1R_2. \tag{2.24}$$

where $\gamma_{th}$ is the threshold gain coefficient and is the gain required to just balance the total losses (such as absorption and scattering in the gain medium, and transmission through the mirrors). Re-arranging we get:

$$\gamma_{th} = \alpha - (1/2L)ln(R_1R_2) \tag{2.25}$$

Resonators

The most widely used laser resonators have either plane or spherical mirrors of rectangular (or, more often, circular) shape, separated by some distance L. Typically, L may range from a few centimeters to a few tens of centimeters, while the mirror dimensions range from a fraction of a centimeter to a few centimeters. Laser resonators thus differ from those used in the microwave field in two main respects: (1) The resonator dimensions are much greater than the laser wavelength. (2) Resonators are usually open, i.e. no lateral surfaces are used. The resonator length is usually much greater than the laser wavelength because this wavelength usually ranges from a fraction of a micrometer to a few tens of micrometers. A laser cavity with length comparable to the wavelength would then generally have too low a gain to allow laser oscillation. Laser resonators are usually open because this drastically reduces the number of modes which can oscillate with low loss.

Of the various possible resonators we make particular mention of the following types: 1. Plane-parallel (Fabry-Perot) resonator $R_1 = R_2 = \infty$ This consists of two plane mirrors set parallel to one another.

2. Spherical cavity resonator $R_1 = R_2 =$ L/2 This consists of two spherical mirrors having the same radius R and separated by a distance L such that the mirror centers of curvature $C_1$ and $C_2$ are coincident (i.e. L = 2R). his type of cavity produces a diffraction-limited beam waist in the centre of the cavity, with large beam diameters at the mirrors, filling the whole mirror aperture. Similar to this is the hemispherical cavity, with one plane mirror and one mirror of radius equal to the cavity length.

3. Confocal cavity resonator $R_1 = R_2 =$ L This design produces the smallest possible beam diameter at the cavity mirrors for a given cavity length, and is often used in lasers where the purity of the transverse mode pattern is important.

4. Concave-convex resonator $R_1 > L$, $R_2 > L$ This design produces no intracavity focus of the beam, and is thus useful in very high-power lasers where the intensity of the intracavity light might be damaging to the intracavity medium if brought to a focus.

For any resonant system, and in particular for a resonant optical cavity, one defines the cavity Q factor (usually abbreviated to cavity Q) as Q=2 (energy stored)/(energy lost in one cycle of oscillation). The quality factor or 'Q' of an inductor or tuned circuit is often used to give an indication of its performance in a resonator circuit. The Q or quality factor is a dimensionless number and it describes the damping in the circuit. It also provides an indication of the resonators bandwidth relative to its centre frequency. The concept of Q, Quality Factor was first envisaged by an engineer named K. S. Johnson from the Engineering Department of the Western Electric Company in the US. He was evaluating the performance and quality of different coils. Over the course of his investigations he developed the concept of Q. Interestingly his choice of the letter Q was made because all other letters of the alphabet were taken and not because of the term quality factor, although with hindsight the choice of the letter Q for quality factor could not have been

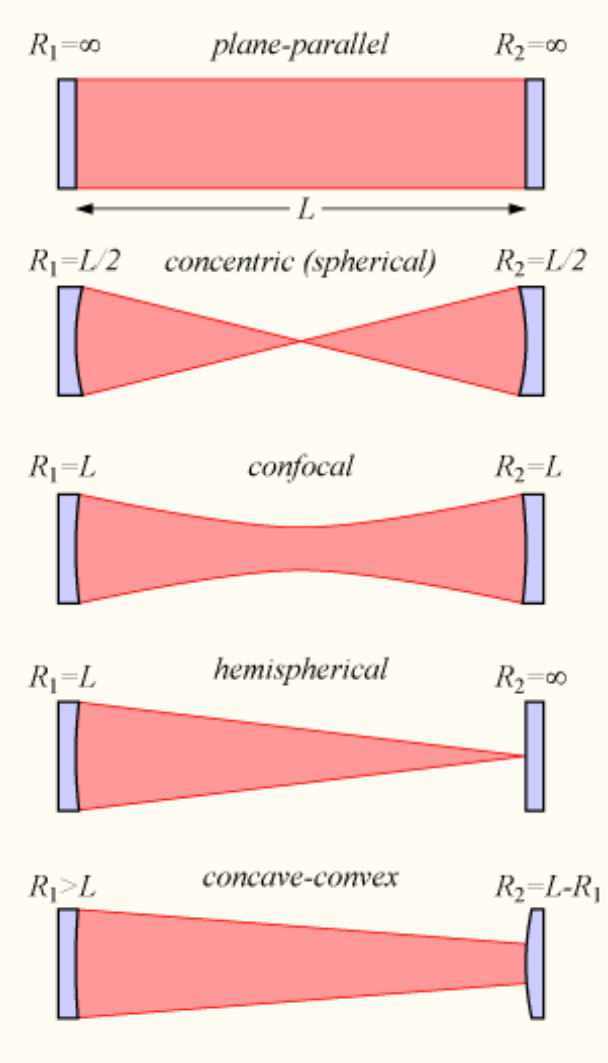


Figure 2.13: Types of two-mirror optical cavities, with mirrors of various curvatures, showing the radiation pattern inside each cavity.

any better. The Q factor is a dimensionless parameter that indicates the energy losses within a resonant element which could be anything from a mechanical pendulum, an element in a mechanical structure, or within electronic circuit such as a resonant circuit.

$$Q = \frac{\lambda}{\Delta\lambda} \tag{2.26}$$

$\lambda$ is the wavelength of the resonance maximum $\Delta\lambda$ is the resonator width or full width at half maximum

Limitation for different materials at different quality factors due to the losses in the materials (the less losses  the higher quality factor).

$$1/Q = 1/Q_{nr} + 1/Q_r \tag{2.27}$$

$Q$ the total quality factor of the resanator

$Q_{nr}$ non-radiative contributions to quality factor

$Q_r$ radiative contributions to quality factor (the first channel is leakage, the second channel is roughness)

Basic equations for lasing

If we consider the population of electron-hole pairs which we generate due to intraband transition

Density of e-h pairs

$$\frac{\partial n}{\partial t} = \eta_p \frac{P}{\hbar\omega_p V_\alpha} - R_{nr}(n) - R_{sp}(n) - R_{st}(n)s). \tag{2.28}$$

Photon density in the cavity mode (kinetic equation for lasing photons)

$$\frac{\partial s}{\partial t} = -\frac{s}{\tau_p} + \Gamma\beta_{sp}R_{sp}(n) + \Gamma R_{st}(n)s. \tag{2.29}$$

In case this speed is negative we have absorption

Life-time of photons in lasing mode

$$\tau_p = Q/\omega. \tag{2.30}$$

Gain

$$g(n) = g_0 ln(\frac{n + N_s}{N_t r + N_s}). \tag{2.31}$$

Rates

Spontaneous emission

$$R_{sp} = n/\tau_{sp}, \tag{2.32}$$

Stimulated emission

$$R_{st} = \nu_g g(n), \tag{2.33}$$

P is the power of incident light, $\eta_p$ is the coupling coefficient, $V_\alpha$ is the volume of mode, $R_{nr}$ is the non-radiative recombination due to some trapping by defects in the system, $s/\tau_p$ is the relaxation or absorption

## 2.2 Basic properties of laser emission

There are some properties which characterise the laser emission such as: high degree of monochromaticity, coherence, directionality, brightness, and short time duration. Let's consider some of them in more details.

Monochromaticity

Light calls monochromatic in case the laser emits all photons with the same energy and the same wavelength (has a single spectral color).

Unfortunatelly, the laser light can not be truly monochromatic, because it requires a wave train of infinite duration. The spectral emission line from which it originates does have a finite width, because of the Doppler effect of the moving atoms or molecules from which it comes. Compared to the ordinary sources of light, the range of frequency (line width) of the laser is extremely small. This range is called line width or bandwidth.

Following are the factors responsible for making the laser beam monochromatic:

1. Only a electromagnetic wave of frequency $\nu_0 = E_2$-$E_1$ only can be amplified, $\nu_0$ has a certain range which is called linewidth, this linewidth is decided by homogeneous broadening factors and inhomogeneous broadening factors

2. The generation of laser is such that the laser cavity forms a resonant system and laser oscillation is sustained only at the resonant frequencies of the cavity. This leads to the further narrowing of the laser line width.

The degree of monochromoticity can be quantitatively described in terms of wavelength bandwidth or frequency bandwidth. The narrower is the line width, higher degree of the monochromocity of the laser has. However this depends on the type of laser, and special techniques can be used to improve monochromaticity. Typically, the frequency bandwidth of a commercial He-Ne laser is about 1500MHz (full width at half-maximum, FWHM). In terms of wavelength, it means that at a wavelength of 632.8nm this means a wavelength bandwidth of about 0.01nm.

Coherence

Apart from spontaneous emission, an excited atom can be induced to emit a photon by another photon of same frequency - i.e. a passing photon can stimulate a transition from a higher level to the lower level, thus resulting in the emission of two photons, which is gain. The two emitted photons are said to be in phase, which means that the crest or the trough of the wave associated with one photon will occur at the same time as on the wave associated with the other photon. An avalanche of similar photons is created and these photons have a fixed phase relationship with each other. This fixed phase relationship between the photons from various atoms in the active medium results in the laser beam generated having the property of coherence. Since the radiation emitted is by the stimulation process, it is referred to as the stimulated emission and the generation of laser is by stimulated emission.

Coherence is a property of waves that indicates the ability of the waves to interfere with each other. Two waves that are coherent can be combined to produce an unmoving

distribution of constructive and destructive interference (a visible interference pattern) depending on the relative phase of the waves at their meeting point.

Using Michelson Interferometer, one can estimate the coherence length by measuring the maximum path difference between the two beams, which still show the interference pattern.

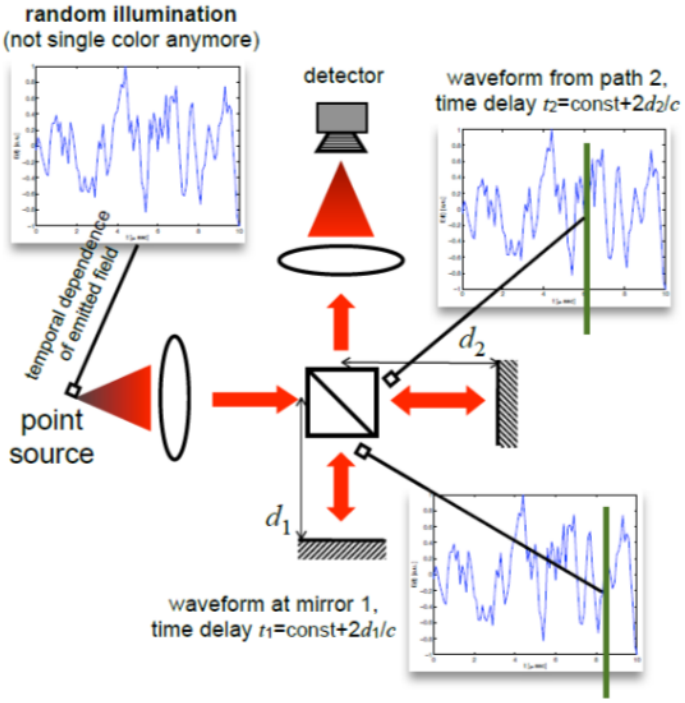


Figure 2.14: M
ichelson interferometer

Temporal coherence

Correlation between the waves at one place at different times, or along the path of a beam at a single instant, are effectively the same thing, and are called temporal coherence. Let us consider a single point on the wave front. There will be a phase difference between time, t = 0 and t = dt of the electromagnetic wave. If this phase difference remains same for any value of dt, then we say that the EM wave has perfect temporal coherence. But if this is only for a specific value of dt, then the EM wave has partial temporal coherence.

If a wave is combined with a delayed copy of itself, the duration of the delay over which it produces visible interference is known as the coherence time of the wave, $\tau_{coh}$. From this, a corresponding coherence length $L_c$, can be estimated as:

$$L_c = c\tau_{coh} = c/(\pi\Delta\omega). \tag{2.34}$$

Homogeneous broadening

A line-broadening mechanism is referred to as homogeneous when it broadens the line of each atom in the same way. In this case the line-shape of the single-atom cross section and that of the overall absorption cross section would be identical. There is some internal mechanism of broadening in each atom. Each atom feels the same broadening mechanism, because broadening is cause by some collisions. All atoms emit the same spectrum with the same center frequency $\nu_0$. Single mode lasing output. Examples of lasers: $Nd^3+$, YAG, phonon collision. Pressure broadening in $CO_2$ lasers.

Inhomogeneous broadening

A line-broadening mechanism is said to be inhomogeneous when it distributes the atomic resonance frequencies over some spectral range. Such a mechanism thus broadens the overall line of the system without broadening the lines of individual atoms. Different atoms emit at slightly differing central frequencies, due to random processes shifting the peak frequency. Each atom is oscillator and it results in Lorance shape for each atom. Multi-mode or single mode lasing output. Examples of lasers: He-Ne lasers, Doppler broadening, Nd3-: glass lasers, amorphous structure broadening.

Spatial coherence

Let us take two points on a wave front, at time equal to zero. There will be a certain phase difference between these two points and if it remains same even after lapse of a period of time, then the electromagnetic wave (em) has perfect coherence between the two points. In case, the phase difference remains same for any two points anywhere on the wave front, then we say that the electromagnetic wave has perfect spatial coherence, where as if this is true only for a specific area, then the electromagnetic wave is said to have only partial spatial coherence. Spatial coherence is related to directionality and uniphase wave fronts. Some randomness in the phase in the space, because of random emission of of light source within one source. Two sources of light for splitting light. Select two places in the wave front frim random wave and measure again signal coming from point and you will see typical interference pattern. The distance between x1 and x2, the less this distance the more chance to have coherent behavior. Spatial coherence is high for sphere waves and plane waves, and is related to the size of the light source. A point source emits spatially coherent light, while the light from a finite source has lower coherence. Spatial coherence can be increased with a spatial filter; a very small pinhole preceded by a condenser lens. The spatial coherence of light will increase as it travels away from the source and becomes more like a sphere or plane wave. Light from distant stars, though far from monochromatic, has extremely high spatial coherence. Coherence length is defined as the length over which energy in two separate waves remains constant. With respect to the laser, it is the greatest distance between two arms of an interferometric system for which sufficient interferometric effects can be observed.

For random source:

$$r_c \sim \frac{\lambda z}{a}. \tag{2.35}$$

$z$ - distance to the source, a - size of the source

For laser:

$$r_c = R. \tag{2.36}$$

R beam radius

Directivity

Another advantages besides coherence is directivety. Laser beam is highly directional, which implies laser light is of very small divergence. This is a direct consequence of the fact that laser beam comes from the resonant cavity, and only waves propagating along the optical axis can be sustained in the cavity. The directionality is described by the light beam divergence angle.

For perfect spatial coherent light, a beam of aperture diameter D will have unavoidable divergence because of diffraction. From diffraction theory, the divergence angle $\theta$ is:

$$\theta = \frac{\beta\lambda}{D}. \tag{2.37}$$

Where $\lambda$ and D are the wavelength and the diameter of the beam respectively. The factor $\beta$ is a numerical coefficient of the order of unity whose value depends on the shape of the amplitude distribution and on the way in which both the divergence and the beam diameter are defined.

If the beam is partial spatial coherent, its divergence is bigger than the diffraction limited divergence. In this case the divergence becomes:

$$\theta_{pc} = \frac{\lambda}{S(1/2)}. \tag{2.38}$$

where S is the coherence area.

Duration

Laser pulse duration is the time during which the laser output pulse power remains continuously above half its maximum value. The optical power appears in pulses of some duration at some repetition rate.

The duration of optical pulses (also called pulse width or pulse length) can vary in a huge range:

1. Infinite continuous-wave lasers ($t = \infty$)

Continuous-wave lasers produce a continuous, uninterrupted beam of light, ideally with a very stable output power.

2. Mechanical shatter ($t > 1$ $\mu$s)
3. Q-switching: Pockels cell ($t > 0.1$ ns)
4. Mode-locking ($t > 1$ fs)

$$sin(\omega_1 t) + sin(\omega_2 t) + ... + sin(\omega_n t) > \beta(t). \tag{2.39}$$

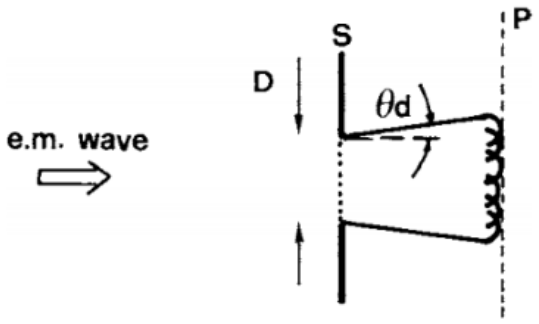


Figure 2.15: Divergence of a plane EM wave due to diffraction. A monochromatic beam of uniform intensity and plane wave-front is assumed to be incident on a screen $S$ containing an aperture $D$. According to Huyghens principle the wave-front at some plane $P$ behind the screen can be obtained from the superposition of the elementary waves emitted by each point of the aperture. We thus see that, on account of the finite size $D$ of the aperture, the beam has a finite divergence $\theta_d$.

extremely short pulse from continuous wave (CW) regime due to synchronization.

It is possible to produce light pulses whose duration is roughly equal to the inverse of the linewidth of the 2 to 1 transition.

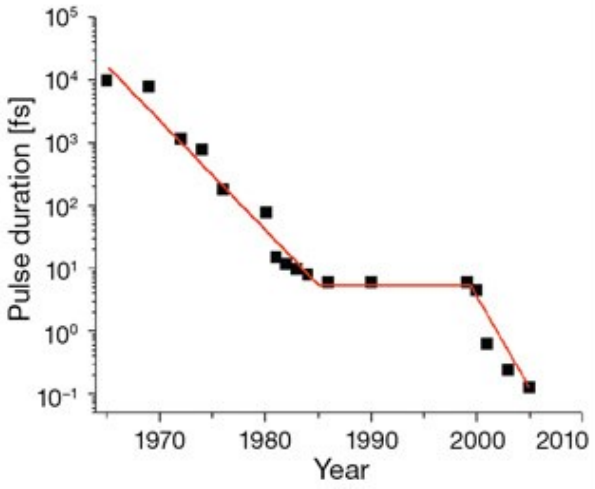


Figure 2.16: Minimum duration of achievable laser-like pulses over time

Basic characteristics of pulsed laser

Pulsed lasers are versatile tools for the scientist and engineer that have played an important role in the development of modern optical physics. The first laser, invented by T, H. Maiman, was a pulsed laser. In this laser a ruby crystal (chromium-doped sapphire) served as the gain medium, which was excited by light from a pulsed flashlamp that surrounded the crystal. Two parallel faces of the crystal were coated with silver, which

served to trap photons emitted along the optic axis so that they would pass through the crystal many times before escaping. The laser operated at room temperature and produced pulses of light with a wavelength of 694 nm (near infrared).

1) Pulse duration (s) - $\tau$
2) Repetition rate (Hz) RR (reversed distance between pulses)
3) Energy per pulse (J) E (how many photons in the pulse)
4) Average power (W) $P_{av}$ (how many energy for period of time)

$$P_av = ERR. \tag{2.40}$$

5) Peak power (W) - $P_{peak}$ (power in each laser pulse)

$$P_peak = E/\tau. \tag{2.41}$$

6) Beam size (cm) D
7) Fluence (J/$m^2$) F

$$F = E/S = \frac{4E}{(\pi D^2)}. \tag{2.42}$$

8) Intensity (W/cm2) I

$$I = F/\tau. \tag{2.43}$$

9) Average intensity (W/cm2)

$$I = WRR. \tag{2.44}$$

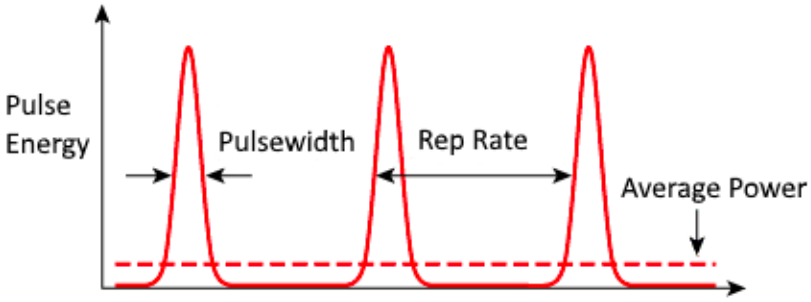


Figure 2.17: Characteristics of pulsed laser. Pulsed lasers emit bursts of light, spaced in time. There is no emission between pulses.

Scale of laser intensities

For laser physics it is a big challenge to shrink light in time scale (to make it short as possible), shrink it in spatial dimension (to focus it as tight as possible) and increase energy.

$$I \sim \frac{E}{D^2 \tau}. \tag{2.45}$$

The International Center for Zetta- and Exawatt Science and Technology (IZEST), a new concept proposed by the French atomic energy commission (CEA) and the cole Polytechnique in September 2011, would provide a fresh impulse to large-scale laser infrastructure projects and reaffirm their importance (see Figure 2...).

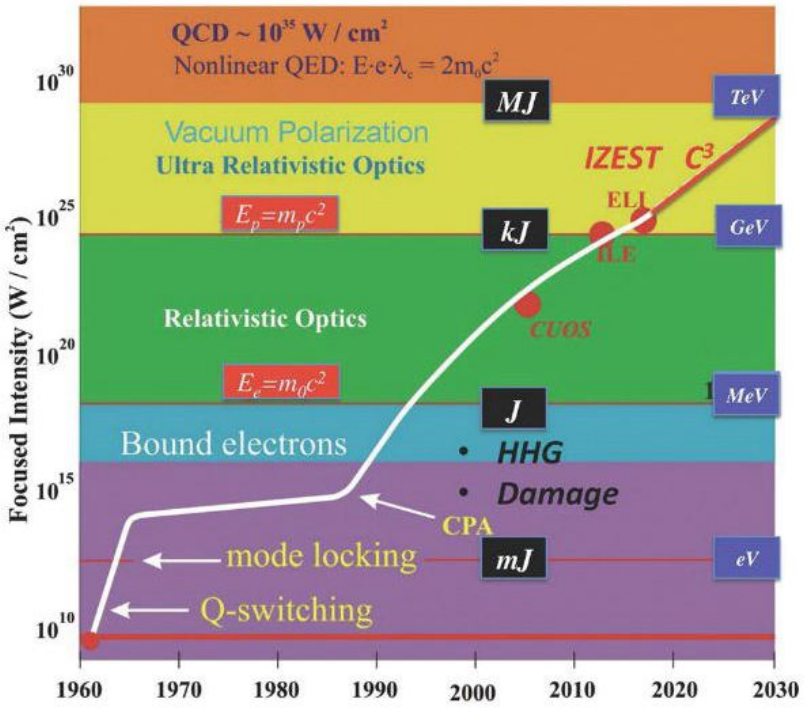


Figure 2.18: Intensity evolution since the first laser demonstration in 1960, with the different regimes of optics and electrodynamics. Red part of line represents the regime addressed by the proposed International Center for Zetta- and Exawatt Science and Technology (IZEST). Black boxes (joules) indicate typical laser energies. Blue boxes (electron volts) indicate typical laser-plasma accelerated particle energies. (QCD, quantum chromodynamics; QED, quantum electrodynamics; E, electric field; e, electron charge; c, compton wavelength; m0, electron mass; c, speed of light. Ep, proton energy; mp, proton mass. Ee, electron energy; C3, cascaded conversion compression; ELI, extreme light infrastructure; ILE, institut de la lumiere extreme; CUOS, Center for Ultrafast Optical Science University of Michigan; HHG, high harmonic generation; CPA, chirped pulse amplification).

# Referenses

1. Svelto O., Hanna D. C. Principles of lasers. New York : Plenum press, 1998. . 4.

2. Kasap S., Capper P. (ed.). Springer handbook of electronic and photonic materials. Springer, 2017.

3. Shaklee K. L., Leheny R. F. Direct determination of optical gain in semiconductor crystals //Applied Physics Letters. 1971. . 18. . 11. . 475-477.

4. Dal Negro L. et al. Applicability conditions and experimental analysis of the variable stripe length method for gain measurements //Optics communications. 2004. . 229. . 1-6. . 337-348.

5. Hill, M.T. and Gather, M.C., 2014. Advances in small lasers. Nature Photonics, 8(12), p.908.

[http://www.spie.org/newsroom/4221-exploring-fundamental-physics-at-the-highest-intensity-laser-frontier?highlight=x2404ArticleID=x88664SSO=1 ] (Courtesy G. Mourou.)

# Chapter 3

# Short and Ultrashort Laser Pulses

# Chapter 4

# Micro- and nanolasers

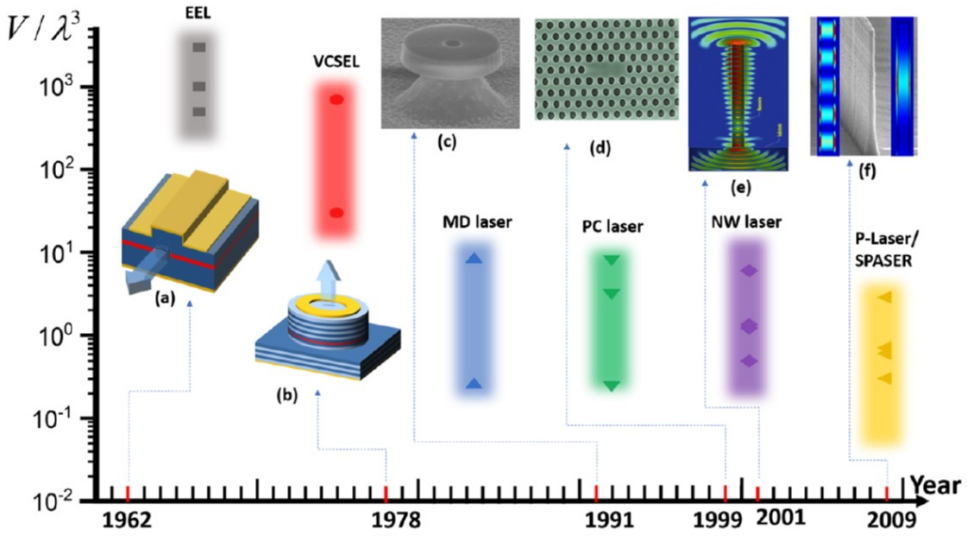


Figure 4.1: Device volume normalized by the wavelength cubed for several types of semiconductor lasers: EEL, edge emitting lasers; MD, microdisk; P-laser, plasmonic lasers. Symbols represent typical values for these lasers; colored bars indicate the ranges of values found in the literature. Red marks along the x axis indicate the years when the type of laser was first experimentally demonstrated. The yellow bar is extended intentionally downward beyond the data symbols to indicate the potential for further size reduction for plasmonic laser and spaser.

## 4.1 Vertical Cavity Surface Emitting Lasers

VCSELs, which are one of the most important types of microsize lasers, were invented many years after the initial demonstration of conventional EELs. VCSELs offer a size reduction of at least an order of magnitude in total device volume compared to EELs (see

Fig.4.1). Currently, VCSELs are one of the most energy-efficient types of lasers that are deployed in practical applications. Even though VCSELs as energy efficient as 50 fJ/bit have been demonstrated in research laboratories, those deployed in practice are much less energy-efficient. Typical VCSELs have diameters of 2 $\mu$m to 10 $\mu$m with a total DBR thickness of 5 $\mu$m to 10 $\mu$m, resulting in a total device volume of 10 to 100 times the wavelength cubed, although the modal volumes are much smaller. Further significant reduction in sizes and energy usage are difficult to achieve because of the poor heat dissipation through thick DBR mirrors and the poor lateral confinement of the VCSEL structures. Thus, it is very difficult for VCSELs to meet the long-term requirements of the size and energy-efficiency challenge for on-chip applications, despite great improvements in recent years.

## 4.2 Microdisk Lasers

Microdisk lasers were initially developed2830 in attempts to miniaturize semiconductor lasers for integrated photonics applications using a free-standing piece of semiconductor based on whispering-galley modes due to the high contrast of refractive indices between semiconductor and air. Such index contrast provides the strongest mode confinement realistically possible without the use of metals or thick DBRs. The unique structures allowed much smaller lasers than possible at the time. The initial devices had diameters between 3 $\mu$m and 5 $\mu$m with a thickness of approximately one micron, resulting in a total device volume of several times the wavelength cubed. Recent work combining the photonic crystal (PC) structure with a microdisk allowed a total device volume of only a small fraction of a wavelength cubed, one of the smallest total volumes achieved (see Fig.4.1). Significant progress has also been made recently in demonstrating micro- or nano-disk lasers using perovskites. Even though perovskites show remarkable optoelectronic properties and may find many interesting applications elsewhere, their use for on-chip interconnects is hindered by several issues such as incompatibility with traditional microfabrication and the lack of perovskites that emit at near-infrared communication wavelengths (e.g., ¿850 nm).

## 4.3 Nanowire Laser

Semiconductor nanowires or nanopillars in air provide one of the best semiconductor optical cavities via the large index contrast (similar to that of microdisk lasers). As with the microdisk lasers, the mode confinement is much better than in typical double- heterostructures, with the possibility of achieving a confinement factor of ¿1. Such nanowires with the two ends exposed to air provide a unique structure both for high-reflective laser cavity and a gain medium at the same time, an ideal combination for laser miniaturization. After the initial wave of laser demonstration in the UV and visible wavelength regime, the first near IR lasing45 was demonstrated using a single GaSb nanowire at the telecom wavelengths. Recently, several realizations of lasing were demonstrated in the short

wavelength NIR regime. To date, almost all of these demonstrations of nanowire lasing were achieved under optical pumping, with only one exception. The ranges of volumes of nanowire lasers are currently comparable to those of microdisk lasers and PC lasers (see Fig.4.1), with the total size as small as twice the wavelength cubed in the IR range. However, further miniaturization of nanowires is possible. One additional advantage of nanowire lasers is the combined material and bandgap flexibility, which allows realization of lasers at wavelengths that are difficult to achieve using either the microdisk approach or the PC approach.

## 4.4 Laser rate equations and $\beta$-factor

The rate equations are a standard and widely used method in studying both the steady state and dynamical behavior of a laser. For nanolasers, however, extra care needs to be applied. For example, the Purcell effect, which characterizes the change of spontaneous emission rate in a subwavelength cavity with respect to that in free space, needs to be incorporated into the rate equations; the normalization of the optical field needs to be calculated properly; and the dispersive nature of materials – especially metal, which is often used in the vicinity of the optical mode in nanolaser design – needs to be considered. Taking these points and the carrier density dependence of the various parameters into account, the rate equations can be written as

$$\frac{\partial n}{\partial t} = \eta_i \frac{I}{qV_a} - R_{nr}(n) - R_{sp}(n) - R_{st}(n)S \tag{4.1}$$

$$\frac{\partial S}{\partial t} = -\frac{S}{\tau_p} + \Gamma_E \beta(n) R_{sp}(n) + \Gamma_E R_{st}(n)S \tag{4.2}$$

where n – carrier density, I – injection current (A), $\eta_i$ – current injection efficiency, $q$ – electron unit charge, $V_a$ – active volume, $R_{nr}(n)$ – non-radiative recombination rate, $R_{sp}(n)$ – total spontaneous emission rate, $R_{st}(n)$ – stimulated emission coefficient, $S$ – photon density, $(n)$ – spontaneous emission coupling factor, $\tau_p$ – photon lifetime and $\Gamma_E$ – energy confinement factor.

In different variations of rate equations, the confinement factor $\Gamma$ has referred to power confinement, electric field confinement, electric energy confinement, and total optical energy confinement. The non-radiative recombination consists of trap-assisted recombination that dominates below threshold and Auger recombination that dominates far above threshold. There are:

$$R_{nr} = An + Cn^3 \tag{4.3}$$

where A is non-radiative recombination constant and C is Auger recombination constant.

The photon lifetime $\tau_p$ is related to the mode wavelength and $Q$ factor:

$$\frac{1}{\tau_p} = \frac{\omega_k}{Q} \tag{4.4}$$

where $\omega_k$ is resonant angular frequency of the $k$-th mode

The total spontaneous emission rate $R_{sp}(n)$ consists of spontaneous emission from all discrete cavity modes, in addition to the radiation into the free space continuum of modes. It is expressed as:

$$R_{sp}(n) = \sum_{k=1} R_{sp,k}(n) + \sum_{k\neq 1} R_{sp,k}(n) + \frac{1}{\tau_{sp,rad}} \int d\mathrm{K} f_{c,\mathrm{K}} \left(1 - f_{v,\mathrm{K}}\right) \tag{4.5}$$

where $k = 1$ denotes the lasing mode, and $k \neq 1$ denotes all other cavity modes. The last term in Eq.4.4 accounts for the radiation into the free-space continuum of modes, and it can be modeled as the ratio between the carrier recombination from active mediums available density of states and the background radiative time $\tau_{sp,rad}$. Last, the single mode spontaneous emission rate $R_{sp,k}(n)$ is related to the total spontaneous emission rate $R_{sp}(n)$ via

$$R_{sp,k}(n) = \beta(n) \cdot R_{sp}(n) \tag{4.6}$$

In Eq.4.4, the carrier density dependency of $\beta$ results from the Purcell effect that is pump dependent: it rises with increasing carrier density until the threshold condition is reached. In the literature, however, the $\beta$-factor is usually taken to be independent of the carrier density.

The cavity Purcell factor $F_p$ is defined as the ratio of spontaneous emission in a cavity to that in free space.

$$F_p \equiv \frac{\tau_{bulk}}{\tau_{cav}} \approx \left[\frac{3}{4\pi^2}\frac{Q}{V_a}\left(\frac{\lambda}{n}\right)^3\right] \tag{4.7}$$

$F_p$ may be large in small laser cavities due to its inverse proportionality to the active region volume $V_a$. However, $F_p$ is actually inversely proportional to the effective size of the mode $V_a/\Gamma_k$, where the mode-gain overlap factor $\Gamma_k$ describes the spatial overlap between the mode and the active region. Thus, if the mode is poorly confined, $\Gamma_k \ll 1$, $F_p$ will remain small, despite a small active region.

We note that the Purcell factor $F_p$ is the sum of contributions $F_{p,mnp}$ from each cavity mode present. Since the $F_p$ is positively related to the modulation speed of a device, it is an important figure-of-merit in designing high-speed lasers.

Because greater emission into the mode that would ultimately lase is generally desirable as it helps utilize the carriers more efficiently, whereas emission into other modes is wasteful. From this point of view, therefore, the appropriate figure of merit is not the Purcell factor $F_{p,mnp}$ but the spontaneous emission factor $\beta$:

$$\beta = \frac{P_{P,\text{lasing}}}{\sum_{mnp} P_{P,\text{map}} + \zeta} \leq \frac{P_{P\text{lasing}}}{\sum_{\text{mop}} P_{P,\text{map}}} = \frac{F_{\text{Plasing}}}{\sum_{\text{mop}} F_{P,\text{mmp}}} \tag{4.8}$$

where the summation is over all cavity modes, and $\zeta$ is the probability of spontaneous emission into free space. The value of $\beta$ is brought closer to its theoretical limit $\beta = 1$ when one summation term is increased and other terms are suppressed, for example, by eliminating unwanted cavity modes, and $\zeta$ is minimized.

At steady state, the photon density $S$ is solved from Eq.4.4-4.4:

$$S = \frac{\Gamma_E \beta(n) R_{sp}(n)}{1/\tau_p - \Gamma_E R_{st}(n)}$$

$\beta$ (and $F_p$)s influence on the light-light curve and the threshold condition is illustrated in Fig.4.2, which plots the light-light curve for different values of $\beta$. Light-light curve is traditionally plotted in linear scale (Fig.4.2), in which a kink is visibly seen for the curve with a small $\beta$ (e.g., $\beta$ of 0.001 and 0.1). This kink is often referred to as the lasing threshold. However, as $\beta$ becomes larger, the kink is gradually replaced by an increasingly smoother feature and eventually completely disappears in the extreme case of $\beta = 1$. While $\beta$ is typically on the order of $1 \cdot 10^5$ for conventional semiconductor lasers, the range of values used in Fig.4.2 is typical for nanolasers. To see more clearly the subthreshold behavior, nanolaser light-light curves are usually plotted in log scale, as shown in Fig.4.2b. Because the kink region is associated with lasing threshold, it is argued that threshold decreases with $\beta$ (all else being equal), and consequently, a thresholdless behavior is reached when $\beta$ becomes unity.

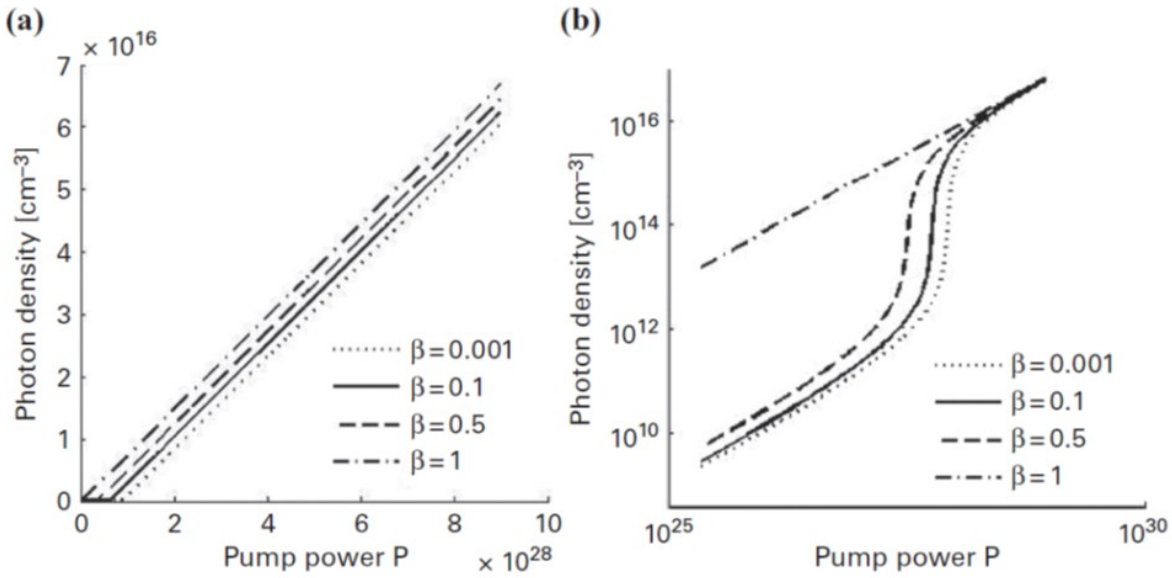


Figure 4.2: Simulated light-in vs. light-out curve for different values of spontaneous emission factor $\beta$, plotted in (a) linear and (b) log scale.

# Chapter 5

# Laser-matter interaction: Light absorption

## 5.1 Optics of metals and semiconductors

Over a wide frequency range, the optical properties of metals can be explained by a plasma model, where a gas of free electrons of number density $n$ moves against a fixed background of positive ion cores. For alkali metals, this range extends up to the ultraviolet, while for noble metals interband transitions occur at visible frequencies, limiting the validity of this approach. In the plasma model, details of the lattice potential and electron-electron interactions are not taken into account. Instead, one simply assumes that some aspects of the band structure are incorporated into the effective optical mass $m$ of each electron. The electrons oscillate in response to the applied electromagnetic field, and their motion is damped via collisions occurring with a characteristic collision frequency $\gamma = 1/\tau$. $\tau$ is known as the relaxation time of the free electron gas.

One can write a simple equation of motion for an electron of the plasma sea subjected to an harmonic external electric field $\mathbf{E}$:

$$m\dot{\mathbf{x}} + m\gamma\ddot{\mathbf{x}} = -e\mathbf{E}_0 e^{-i\omega t} \tag{5.1}$$

Solving this equation with taking into account connection with macroscopic polarization determines dielectric function as:

$$\epsilon'(\omega) = 1 - \frac{\omega_p^2 \tau^2}{\omega^2 + \gamma^2\omega^2} \tag{5.2}$$

$$\epsilon''(\omega) = \frac{\omega_p^2 \tau}{\omega(\omega^2 + \gamma^2\omega^2)} \tag{5.3}$$

where $\omega_p^2 = \frac{ne^2}{\epsilon_0 m}$ is the plasma frequency of the free electron gas.

Whereas our description up to this point has assumed an ideal free-electron metal, we will now compare the model with an example of a real metal. In the free-electron model,

$\epsilon \to 1$ at $\omega >> \omega_p$. For the noble metals (e.g. Au, Ag, Cu), an extension to this model is needed in the region $\omega > \omega_p$ (where the response is dominated by free s electrons), since the filled d band close to the Fermi surface causes a highly polarized environment. This residual polarization due to the positive background of the ion cores can be described by adding the extra-term and dielectric function can be written as:

$$\epsilon(\omega) = \epsilon_\infty - \frac{\omega_p^2}{\omega^2 + i\gamma\omega} \tag{5.4}$$

where $\epsilon_\infty$ corresponds with localised electron polarisation.

The validity limits of the free-electron description 5.1 are illustrated for the case of gold in Fig.5.1. It shows the real and imaginary components $\epsilon'$ and $\epsilon''$ for a dielectric function of this type, fitted to the experimentally determined dielectric function of gold [Johnson and Christy, 1972]. Clearly, at visible frequencies the applicability of the free-electron model breaks down due to the occurrence of interband transitions, leading to an increase in $\epsilon''$.

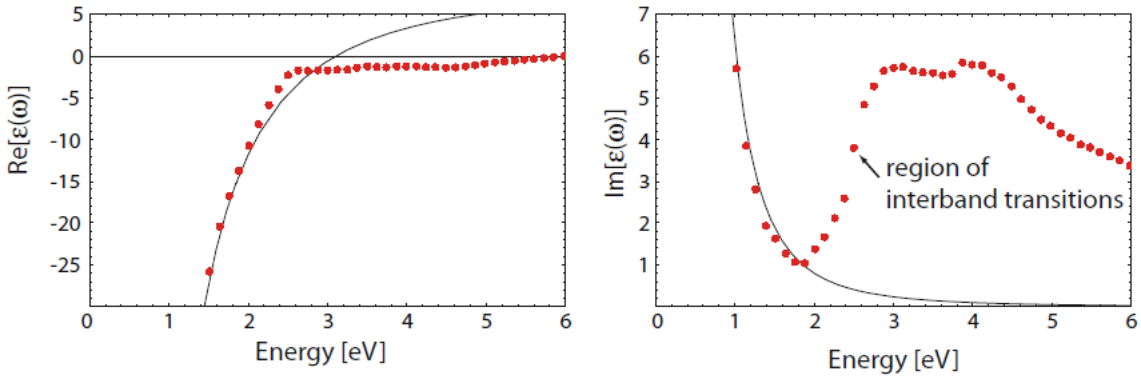


Figure 5.1: Dielectric function $\epsilon(\omega)$ of the free electron gas (solid line) fitted to the literature values of the dielectric data for gold [Johnson and Christy, 1972] (dots). Interband transitions limit the validity of this model at visible and higher frequencies.

## 5.2 Carriers dynamics

Under the action of laser pulsed radiation with an energy density $Q$, a pulse duration $\tau_p$ and photon energy $\hbar\omega$ on the semiconductor surface nonequilibrium carriers are generated due to interband absorption. Equation for nonequlibrium carrier density can be written as:

$$\frac{\partial n_c}{\partial t} = D\frac{\partial^2 n_c}{\partial z^2} + G - R, \tag{5.5}$$

where $D$ is diffusion coefficient, $G$ and $R$ are generation and recombination rates, respectively.

Since the absorption of a single photon from a laser beam is accompanied by the production of one electron-hole pair, the rate of generation of free carriers can be determined by the rate of absorption of energy in the near-surface layer dividing by the photon energy $\hbar\omega$:

$$G(t,z,T) = \frac{\alpha(t,z,T)(1-R)}{\hbar\omega\tau_p} Q exp(-\int_0^Z \alpha(t,z',T)dz') \approx G_0 exp(-\alpha z), \tag{5.6}$$

where $\alpha = \alpha^L + \alpha^{NL}$ is the sum of linear and nonlinear coefficients, T is the temperature and R is optical reflection coefficient.

Auger recombination is a fundamental process of the semiconductor material. It is a band-to-band, three-particle scattering process that involves either: i) an e-e collision in the conduction band and recombination with a hole in the valence band or ii) a h-h collision in the valence band followed by recombination with an electron in the conduction band. Three distinct paths are shown in Fig.5.2: CCCH, CHHS, CHHL, where letter C stands for conduction electron, H for heavy-hole, L for light-hole and S for split-off hole. In CCCH, two electrons in the conduction band and one hole in the heavy hole band are involved. In CHHS, one electron in the conduction band, one hole in the heavy hole band, and one hole in the split off band interact. In CHHL, one electron from the conduction band and two holes in the heavy hole band scatter.

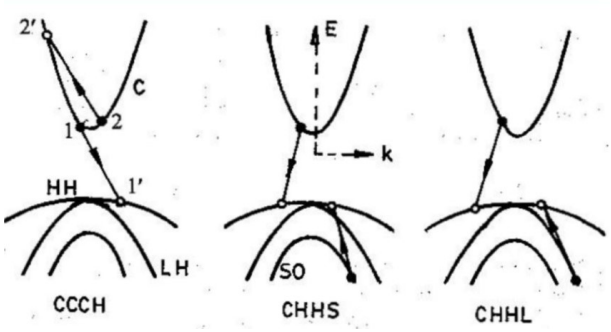


Figure 5.2: E-k diagrams for various Auger recombination processes in a direct bandgap semiconductor.

A collision occurs between two carriers in the same band (e-e or h-h): energy from the recombining carrier is transferred to the remaining carrier. Note that both energy and momentum must be conserved to complete the scattering event. The excited or hot carrier will quickly thermalize with the lattice via phonon emission and generate heat. The Auger recombination process in semiconductors can either be direct or phonon-assisted. The CCCH and CHHS are believed to be the two dominant processes. The net rate of Auger recombination in steady-state can be written as:

$$R_A = C_e \left(n^2 p - n_0^2 p_0\right) + C_p \left(n p^2 - n_0 p_0^2\right), \tag{5.7}$$

where $C_e$ and $C_p$ denote the non-radiative Auger recombination coefficients for electrons and holes, respectively. These coefficient are independent of carrier density. Using the assumptions $n = p = n_c$ the non-radiative Auger recombination rate can be written as:

$$R_A = (C_e + C_p) = C n_c^3, \tag{5.8}$$

where $C$ is the aggregate Auger non-radiative coefficient.

Radiative recombination occurs in direct band semiconductors. Details of this recombination are shown in Fig.5.3. After absorption of photon electron-hole pair are generated. Hot carriers give off heat to phonons and after annihilation electron with hole photon radiates. Radiative recombination rate is proportional concentration of both types of carriers. The radiative recombination rate Using the previous assumptions can be written as:

$$R_r = B n_c^2, \tag{5.9}$$

where constant coefficient B is obtained from a spectral integration of the spontaneous emission rate.

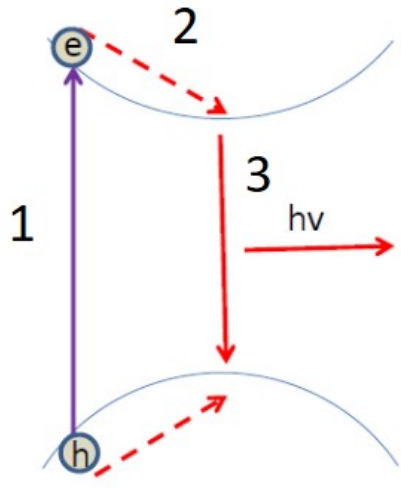


Figure 5.3: E-k diagram of radiative recombination. 1 - absorption: e-h pair generation, 2 - Intraband relaxation: e(h)-phonon scattering and 3 - Interband relaxation: e-h annihilation and photon emission.

Third recombination process is non-radiative trap recombination. Scheme of this recombination mechanism are presented on Fig.5.4. In general rate of this process corresponds with electron and traps concentrations. In simplest case non-radiative rate can be written as:

$$R_{nr} = An_c, \tag{5.10}$$

where A is constant of non-radiative recombination depending on trap cross-section.

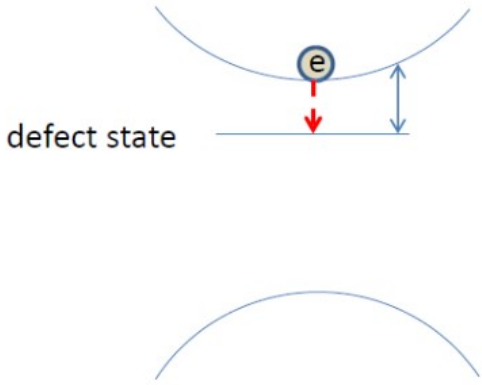


Figure 5.4: Scheme of non-radiative recombination process

Taking into account this three recombination processes, extremely shot duration of laser pulse and neglecting of diffusion Eq.5.2 can be rewritten as:

$$\frac{\partial n_c}{\partial t} = -An_c - Bn_c^2 - Cn_c^3. \tag{5.11}$$

Solving this equation with taking into account all recombination processes is complicated. But variation of power can make distinguishable different contributions. Fig.5.5 present dependence of rates on carrier density. There are three different regions with pronounce domination of different processes: I - nonradiative, II - radiative and III - Auger.

The dominance of different recombination processes depending on the carrier concentration is clearly seen in the time-resolved photoluminescence measurements. Carrier control are available by varying the excitation power. Fig.5.6 demonstrate changes of lifetimes depending on pump intensity.

## 5.3 Principles of Electromagnetic heating

Temperature distributions induced by the absorption of laser radiation have been calculated on the basis of the heat equation. In the most general case, the temperature

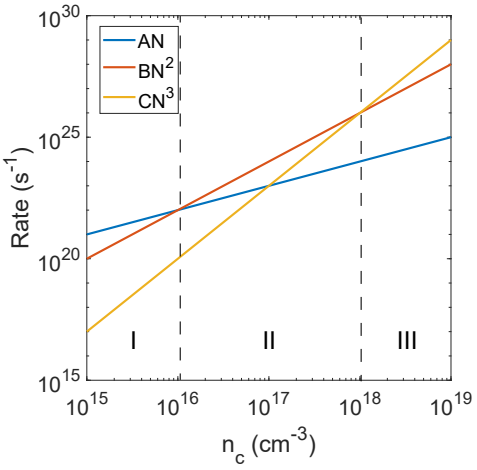


Figure 5.5: Recombination rates: I - nonradiative, II - radiative and III - Auger

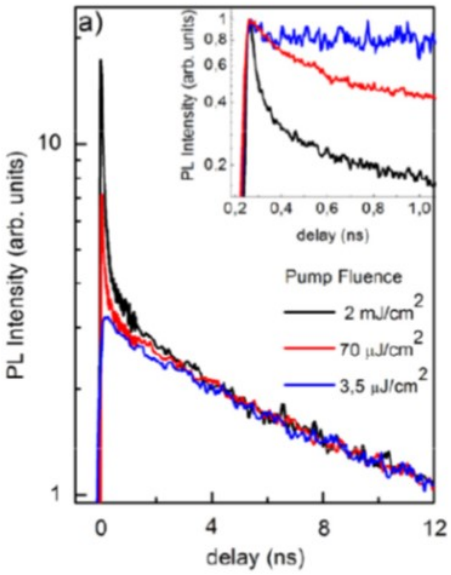


Figure 5.6: Time-resolved measurements for different fluences.

$T = T(x,t) = T(x_\alpha, t)$ is a function of both the spatial coordinates $_\alpha$ and the time $t$. With fixed laser parameters the temperature distribution depends on the optical absorption within the irradiated zone, on the transport of heat out of this zone. In the absence of heat transport by convection and thermal radiation, the heat equation can be written as

$$\rho(T)c_{\mathrm{p}}(T)\frac{\partial T(x,t)}{\partial t} - \nabla[\kappa(T)\nabla T(x,t)] = Q(x,t), \tag{5.12}$$

where $\rho$ is the mass density, $c_p(T)$ is the specific heat at constant pressure, $\kappa$ is thermal conductivity and $Q(x,t)$ is heat source.

For laser beam focused in the spot general from solution Eq.5.3 temperature distribution $T(r) \sim \exp\left(-r^2/L_{\text{tot}}^2\right)$, where $L_{\text{tot}}$ is characteristic width of temperature distribution. This width are determined by diffusion length ($\sim (\tau_{pulse} D)^{(1/2)}$) and depth of penetration of electromagnetic radiation ($\sim \lambda/Im(n)$). It's perfectly clear that for dielectric diffusion length is small because they have a low conductivity and large penetration depth because imaginary part of refractive index is low. For metals it's vice versa: conductivity and imaginary refractive index is high.

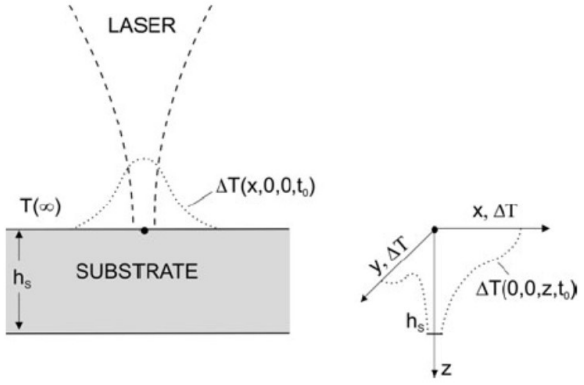


Figure 5.7: Infinite slab of uniform thickness $h_s$ irradiated by a laser beam at perpendicular incidence. The laser-induced temperature rise on the surface $z = 0$ and along the z-direction is indicated (dotted curves). The temperature far away from the irradiated area is $T(\infty)$.

## 5.4 Principles of ultrafast electromagnetic heating

In metals, light is almost exclusively absorbed by freefree electron transitions within the conduction band. Within the electron system, the excitation energy is thermalized within, typically, 10 fs to 1 ps. Thermalization between the electron subsystem and the lattice is much slower, typically of the order of 1100 ps, depending on the strength of electronphonon coupling $\Gamma_{e-ph}$. Thus, femtosecondlaser excitation generates a hot electron gas. The transient non-equilibrium between the hot electrons and the lattice can be described by temperatures $T_e$ and $T$ , which can be calculated from the corresponding heat equations. This description is denoted as the two-temperature model. In the laboratory system, the (coupled) nonlinear equations for $T_e$ and $T$ can be written, in a more general form, as:

$$C_{\text{e}}\left(T_{\text{c}}\right)\frac{\partial T_{\text{e}}}{\partial t} = \nabla\left[\kappa_{\text{e}}\left(T_{\text{e}},T\right)\nabla T_{\text{e}}\right] - \Gamma_{\text{e-ph}}\left(T_{\text{e}}\right)\left[T_{\text{e}} - T\right] + Q\left(x_\alpha, t\right) \tag{5.13}$$

and

$$C(T)\frac{\partial T}{\partial t} = \nabla[\kappa(T)\nabla T] + \Gamma_{\text{e-ph}}\left(T_{\text{e}}\right)\left[T_{\text{e}} - T\right], \tag{5.14}$$

where $C_e$ and $C$ are the heat capacities (per unit volume) of the electron and lattice subsystems, respectively.

The two-temperature model describes the laser excitation of conduction band electrons and the subsequent energy transfer from the hot electrons to the lattice vibrations via the electron-phonon coupling. The model assumes the validity of the heat equation for ultrashort laser pulses. In other words, it assumes that the energy distribution of the electrons is thermalized and can be described by a temperature $T_e$. In many applications of Eqs.5.4-5.4 the coefficients have been assumed as constants. This is, however, inadequate in most cases. The consideration of the influence of the electron temperature Te on the electron-phonon coupling and electron heat capacity, is quite important.

Fig.5.8 shows the temporal dependence of the electron and lattice temperatures calculated from the two temperature model for 100 nm thick films of Au and Ni. These metals are representative examples for weak and strong electron-phonon coupling ($\Gamma_{e-ph}(Au) \approx 2.3 \cdot 10^{10} W/cm^3K; \Gamma_{e-ph}(Ni) \approx 3.6 \cdot 10^{11} W/cm^3K$). The differences in eph are directly revealed in the different behavior of temperatures $T_e$ and $T$ . In particular, the time required to reach thermal equilibrium in Au is almost ten times longer than for Ni. Another consequence is the temperature gradient that builds up between the front and the rear sides. In Au, $\Gamma_{e-ph}$ is small and thus $l_e \approx (D_e C_e/\Gamma_{e-ph})$ large. Therefore, the absorbed energy can spread into deeper parts of the sample and thereby diminishes the energy density in the surface region. Films with a thickness comparable to $l_e$, are heated almost homogeneously. The opposite behavior is found for Ni. Strong electron-phonon coupling causes rapid cooling of the hot electrons and thereby prevents long-range energy transport by electron diffusion.

The two temperature model permits a qualitative and, in certain cases, an even semi-quantitative interpretation of ultrashort-pulse laser-metal interactions. For example, Fig.5.8 explains the differences in damage (melting) thresholds for noble metals and transition metals, and thereby the importance of the electron-phonon coupling. Due to rapid energy transport by hot electrons, the damage threshold observed (experimentally) with Au is higher than for Ni. This agreement also proves the thermal character of laser-metal interactions for fs-laser pulses. It should be noted, however, that with ns-pulses the damage threshold is higher for Ni in comparison to Au.

## 5.5 Ultrafast Optical Techniques

With the development of ultrashort-pulse lasers, fast optical techniques for investigating transient laser-induced phenomena have become of increasing importance. Clearly, the classification between quasistationary diagnostic techniques and ultrafast optical techniques is somewhat arbitrary. Transient laser-induced phenomena are used in temporal evolutions of surface reflectivities, surface deformations, melting, ablation thresholds and other. Schematic picture of an experemental setup for time-resolved microscopy.

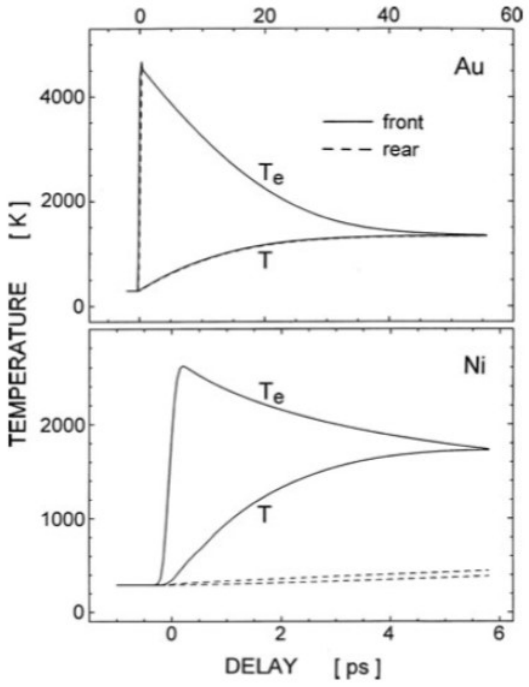


Figure 5.8: Temporal dependence of the electron temperature $T_e$ and lattice temperature $T$ calculated for 100 nm films of Au and Ni irradiated with 200 fs pulses. Solid curves show the temperature at the surface (front side) of films; dashed curves show the temperature at the rear side. With Ni, thermal equilibrium is reached about 10 times faster in comparison to Au

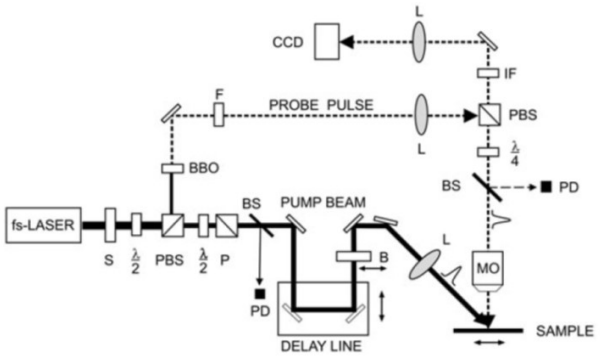


Figure 5.9: An experimental setup employed for fs-time-resolved microscopy. Part of the fs-laser beam is used as a probe beam which is frequency doubled (BBO crystal). The signal reflected from the sample surface is imaged onto a CCD camera. S: electromechanical shutter; PBS: polarizing beam splitter; P: polarizer; BS: beam splitter; L: lens; F: bandpass filter; PD: photodiode;MO: microscope objective; IF: interference filter

# References

1. Maier S. A. Plasmonics: fundamentals and applications. - Springer Science & Business Media, 2007.

2. Koroteev N. I., Shumai I. L. Physics of intense laser radiation. - 1991.

3. Bäuerle D. Laser processing and chemistry. - Springer Science & Business Media, 2013.

4. Chuang S. L. Physics of optoelectronic devices. - 1995.

5. Karpov S. ABC-model for interpretation of internal quantum efficiency and its droop in III-nitride LEDs: a review //Optical and Quantum Electronics. - 2015. - V. 47. - 6. - P. 1293-1303.

# Chapter 6

# Optical Heating for Nanophotonics

## 6.1 Optical Heating Equations

For solving problem of optical heating lets start with general equation for heat problem:

$$\rho c_p \partial T/\partial t = \nabla(\kappa \nabla T) + (\partial Q/\partial t), \tag{6.1}$$

where $\rho$ is material density, $c_p$ is heat capacity, $\kappa$ is thermal conductivity, $T$ is temperature and $Q$ is the amount of heat received per unit volume of material.

In particular solution temperature dependence of $\rho$, $c_p$, $\kappa$ and $(\partial Q/\partial t)$ is negligible in most cases. When for description of hearing Eq.6.1 can be rewritten as:

$$\partial T/\partial t = \chi \Delta T + (\rho c_p)^{-1} (\partial Q/\partial t), \tag{6.2}$$

where $\chi = \kappa/\rho c_p$ is thermal diffusivity.

Laser beam propagation along the axis z and fall on xy plane of material create volume heat source:

$$\partial Q/\partial t = \alpha I(r,t), \tag{6.3}$$

where $\alpha$ is absorption coefficient and $I(r,t)$ is distribution of light intensity (in region z¿0). In simplest case of Gaussian beam expression are obtained:

$$I(r,t) = (1-R) I_0 \exp(-\alpha z) \exp\left[-\left(x^2+y^2\right)/a^2\right] f\left(t/\tau_p\right), \tag{6.4}$$

where $I_0$ is the intensity of radiation incident on the absorbing medium from the outside, $R$ is optical reflection coefficient and $a$ is radius of Gaussian beam. Function $f\left(t/\tau_p\right)$ describes temporal shape of laser pulse with duration $\tau_p$.

Since the Eq.5.3 is linear, it is also valid for the increase of body temperature $T' = T - T_0$, where $T_0$ is body temperature with absent of optical excitation. For definiteness, we will consider the process of heating a material in the absence of heat exchange with the environment using the following boundary condition:

$$-\left. q_z \right|_{z=0} = \chi \left. \frac{\partial T'}{\partial z} \right|_{z=0} = 0 \tag{6.5}$$

The method of green functions is convenient for solving the Eq.5.3. Indeed, lets assume $G\left(r - r', t - t'\right)$ is the solving for heat source localised in $r = 0$ and has instant impulse i.e:

$$\frac{1}{\rho c_p}\left(\frac{\partial Q}{\partial t}\right) \to A\delta\left(\boldsymbol{r} - \boldsymbol{r}'\right)\delta\left(t - t'\right) \tag{6.6}$$

When because Eq.6.1 and boundory conditions Eq.6.1 are linear solving heat problem with arbitrary source has the form:

$$T(r,t) = \frac{1}{\rho c_p}\int_{-\infty}^{t} dt' f\left[\frac{\partial Q}{\partial t}\left(r', t'\right)\right] G(r - r, t - t) d^3 r' \tag{6.7}$$

For point source Eq.6.1 can be rewritten as:

$$\partial T'/\partial t = \chi \Delta T' + A\delta(r)\delta(t) \tag{6.8}$$

Solving this equation with taking into account boundary conditions gives the following expression:

$$T'(r,t) = \frac{A}{(4\pi\chi t)^{3/2}} \exp\left(-\frac{r^2}{4\chi t}\right) \tag{6.9}$$

According this expression after instant point energy uprise the temperature in heat point has temporal low like $T' \sim t^{-3/2}$. And characteristic size of heating area increase $r_0 \sim (\chi t)^{1/2}$.

According all of the above general solution for continuous wave laser excitation can be wtitten as:

$$\frac{\partial T}{\partial t} = \frac{\alpha(1-R)I_0}{2\rho_0 c_p}\frac{1}{1+4\chi t/a^2}\exp\left(-\frac{x^2+y^2}{a^2+4\chi t}\right)\exp\left(\alpha^2\chi t\right)\left\{\exp(\alpha z)\,\mathrm{erfc}\left[\alpha(\chi t)^{1/2} + \frac{z}{(4\chi t)^{1/2}}\right] + \right.$$
$$\left. + \exp(-\alpha z)\,\mathrm{erfc}\left[\alpha(\chi t)^{1/2} - \frac{z}{(4\chi t)^{1/2}}\right]\right\}\theta(t) \quad ,$$

(6.10)

where $\theta(t)$ is Heaviside function and $\operatorname{erfc} x = \frac{2}{\sqrt{\pi}} \int_x^\infty e^{-t^2} \mathrm{d}t$ is complementary error function.

The maximum rate of temperature increase is observed on the surface of the irradiated substance (z=0) on the axis of the laser beam (x=y=0):

$$\frac{\partial T'}{\partial t}(r=0,t) = \frac{\alpha(1-R)I_0}{\rho_0 c_p} \frac{\exp\left(\alpha^2 \chi t\right) \operatorname{erfc}\left[\alpha(\chi t)^{1/2}\right]}{1+4\chi t/a^2} \tag{6.11}$$

According Eq.6.1 at the initial stage ($t \leqslant \min\{a^2/\chi, 1/\alpha^2\chi\}$) thermal conductivity does not affect the heating rate which is constant ($\partial T/\partial t = \alpha(1-R)I_0/\rho_0 c_p$). The physical meaning of the quantity $a^2/\chi$ is the characteristic time during which the influence of the heat source extends to a distance of the transverse size of the laser beam $a$.

Similarly, it can be said that the finiteness of the depth of penetration of light in matter ($d = \alpha^{-1}$ absorption length) will manifest itself in heating only characteristic time later $d^2/\chi = 1/\alpha^2\chi$. Thus at times $t \leqslant \min\{a^2/\chi, 1/\alpha^2\chi\}$ the maximum temperature of a substance increases over time according to a linear law: $T \sim t$.

Let us assume that the transverse size of the laser beam is significantly greater than the absorption length ($a \gg d$). Then, with time increasing the heat transfer into the medium "switch on" of the first time is included which reduces the rate of heating. For condition $1/\alpha^2\chi \leqslant t \leqslant a^2/\chi$ Eq.6.1 takes the form:

$$\frac{\partial T'}{\partial t} \approx \frac{(1-R)I_0}{\rho_0 c_p} \frac{1}{(\pi\chi t)^{1/2}} \sim t^{-1/2} \tag{6.12}$$

Therefore, the temperature increment grows sublinearly ($T \sim t^{1/2}$). Time $t \geq a^2/\chi$ after the laser exposure, thermal conductivity in the direction along the surface begins to influence the temperature increase. Heating rate decreases rapidly. At $ta^2/\chi$ solving is:

$$\left.\frac{\partial T'}{\partial t}\right|_{t\to\infty} \approx \frac{(1-R)I_0 \pi a^2}{\rho_0 c_p (4\pi\chi t)^{3/2}} \tag{6.13}$$

Maximum temperature $T'_{max}$ at $ta^2/\chi$ is established by law:

$$T' = T'_{\max} - \frac{(1-R)I_0\pi a^2}{2\rho_0 c_p \pi\chi(4\pi\chi t)^{1/2}} \tag{6.14}$$

The maximum temperature $T'_{max}$ are defined as integral Eq.6.1: $T'_{max} = T'(r=0, t=\infty$. In case $\alpha a \gg 1$ it can be estimated as:

$$T'_{\max} \sim \frac{(1-R)I_0 a}{\rho_0 c_p \chi} = \frac{(1-R)\mathfrak{P}}{\kappa a}, \tag{6.15}$$

where $\mathfrak{P} = a^2 I_0$ is total power of Gaussian beam with $a$ radius and $I_0$ intensity.

## 6.2 Heating of Nanoparticle

The power absorbed by a nanoparticle (NP) can be simply expressed using the absorption cross-section $\sigma_{abs}$ :

$$Q = \sigma_{\text{abs}} I \tag{6.16}$$

were I is the intensity of the incoming light. In the case of a plane wave $I = n_{\text{s}} c_0 \varepsilon_0 \left|\mathbf{E}_0\right|^2 /2$.

The heat generation can be also derived from the heat power density $q(\mathbf{r})$ inside the NP such that $Q = \int_V q(\mathbf{r}) \mathrm{d}^3 r$, where the integral runs over the NP volume V. Since the heat originates from Joule effects, the heat power density reads

$$q(\mathbf{r}) = \frac{1}{2} \operatorname{Re}\left[\mathbf{J}^\star(\mathbf{r}) \cdot \mathbf{E}(\mathbf{r})\right] \tag{6.17}$$

where $\mathbf{J}(\mathbf{r})$ is the complex amplitude of the electronic current density inside the NP. As $\mathbf{J}(\mathbf{r}) = i\omega\mathbf{P}$ and $\mathbf{P} = \varepsilon_0 \varepsilon(\omega)\mathbf{E}$ one ends up with

$$q(\mathbf{r}) = \frac{\omega}{2} \operatorname{Im}(\varepsilon(\omega)) \varepsilon_0 |\mathbf{E}(\mathbf{r})|^2 \tag{6.18}$$

The heat generation is thus directly proportional to the square of the electric field inside the NP. In practice there are thus two ways of calculating the heat power $Q$ absorbed by a given NP. For geometries for which the absorption cross-section is known (for example for spherical NPs), $Q$ can be estimated using Eq.6.2. However, for more complicated morphologies for which there is no simple analytical expression available, the computation of the inner electric field amplitude $\mathbf{E}(\mathbf{r})$ is required to calculate $q(\mathbf{r})$ from Eq.6.2.

While the computation of the delivered heat power $Q$ turns out to be a full-optical problem as explained in the previous section, the determination of the steady-state temperature distribution $T(\mathbf{r})$ inside and outside the NP is based on the resolution of the heat diffusion equation:

$$\begin{array}{ll} \nabla \cdot [\boldsymbol{\kappa}(\mathbf{r}) \nabla T(\mathbf{r})] = -q(\mathbf{r}) & \text{inside the NP} \\ \nabla \cdot [\boldsymbol{\kappa}(\mathbf{r}) \nabla T(\mathbf{r})] = 0 & \text{outside the NP} \end{array} \tag{6.19}$$

where $\boldsymbol{\kappa}(\mathbf{r})$ is the thermal conductivity. For a spherical NP of radius $R$, simple calculations lead to a temperature increase:

$$\begin{array}{ll} \delta T(r) = \delta T_{\text{NP}} \frac{R}{r}, & r > R \\ \delta T(r) \approx \delta T_{\text{NP}}, & r < R \end{array} \tag{6.20}$$

where $\delta T_{\text{NP}}$ is the temperature increase of the NP. Interestingly, while the heat power density $q(\mathbf{r})$ can be highly non-uniform within the NP, the temperature at equilibrium is,

on the contrary, generally perfectly uniform inside the NP. This is due to the much larger thermal conductivity of material as compared with that of the surroundings (air, glass, etc.). The actual temperature increase experienced by a NP is dependent on numerous parameters, namely its absorption cross-section, its shape, the thermal conductivity of the surrounding medium and the wavelength and irradiance of the incoming light. For a spherical NP, the NP temperature increase is related to the absorbed power $Q = \sigma_{\mathrm{abs}} I$ according to

$$\delta T_{\mathrm{NP}} = \frac{Q}{4\pi\kappa_{\mathrm{s}} R} \tag{6.21}$$

where $\kappa(r)$ is the thermal conductivity of the surrounding medium.

The establishment of this steady-state temperature profile is usually very fast when working with NPs. The typical duration $\tau_{tr}$ of the transient regime is not dependent on the temperature increase but on the characteristic size $L$ of the system (for instance the radius R for a sphere):

$$\tau_{\mathrm{tr}} \sim L^2 \frac{\rho c_{\mathrm{p}}}{3\kappa_{\mathrm{s}}} \tag{6.22}$$

where $\rho$ is the mass density of the NP and $c_p$ its specific heat capacity at constant pressure. For example, for spherical NPs with different diameters in water value of $\tau_{tr}$ are shown on Fig.6.1.

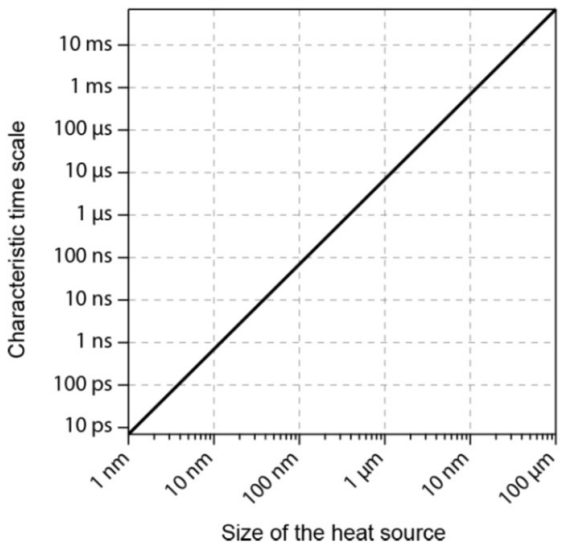


Figure 6.1: Characteristic time scale of heat diffusion in water as a function of the size of the heat source.

The absorption of laser pulse energy by a NP can be described as a three-step process, each of these steps involving different time scales as follows.

During the interaction with the laser pulse, part of the incident pulse energy is absorbed by the gas of free electrons of the NP, much lighter and reactive than the ion lattice. The electronic gas thermalizes very fast , for gold time scale $\tau_e$=100 fs. This leads to a state of non-equilibrium within the NP: the electronic temperature Te of the electronic gas increases while the temperature of the lattice (phonons) $T_p$ remains unchanged.

Subsequently, this hot electronic gas relaxes (cools down), through internal electron-phonon interaction characterized by a time scale $\tau_{e-ph}$ to thermalize with the ions of the gold lattice. This time scale is not dependent on the size of the NP except for NPs smaller than 5 nm due to confinement effects. Above this size and for moderate pulse energy, the time scale is constant and equals $\tau_{e-ph}$= 1.7 ps for gold. At this point, the NP is in internal equilibrium at a uniform temperature ($T_e = T_p$), but is not in equilibrium with the surrounding medium that is still at the initial ambient temperature.

The energy diffusion from the NP to the surroundings usually occurs at longer characteristic time scale $\tau_{tr}$ (see Eq.6.2) and leads to a cooling of the NP and a heating of the surrounding medium.

During this process, the total absorbed energy reads as $\sigma_{\mathrm{abs}}\langle I\rangle/f = \sigma_{\mathrm{abs}}F$ where $f$ is the pulsation rate and $F$ the fluence of the laser pulse. Different regimes can be observed depending on the pulse duration compared with $\tau_{tr}$. When the pulse duration is short enough and/or the NP is small enough, the three steps can be considered to happen successively. In this regime, the initial temperature increase reaches its maximal value:

$$\delta T_{\max} = \frac{\sigma_{\mathrm{abs}}\langle I\rangle}{V\rho c_{\mathrm{p}} f} = \frac{\sigma_{\mathrm{abs}}F}{V\rho c_{\mathrm{p}}} \tag{6.23}$$

where $V$ is the volume of the NP.

The thermodynamics is also influenced by the pulsation rate $f$ of the laser. If $f$ is too high, the particle may not have time to completely cool down between two successive pulses. This leads to a regime where the NP is permanently hot, as seen in Fig.6.2. In practice, such a regime is achieved when $f > 1/\tau_{tr}$ discriminate between both regimes, a dimensionless number $\xi$ can be introduced such that $\xi = f\tau_{tr}$. For $\xi \ll 1$ , a temperature confinement can be expected and is subject to the following law:

$$T(r,t) = \frac{\sigma_{abs}F}{c_{\mathrm{ps}}\rho_{\mathrm{s}}} \frac{1}{(4\pi D_{\mathrm{s}}t)^{3/2}} \exp\left(-\frac{r^2}{4D_{\mathrm{s}}t}\right) \tag{6.24}$$

Otherwise, an extended temperature dependence like Eq.6.2 be dominant. Comparison of this two regimes are presented on Fig.6.3. Where also temporal evolution of temperature are shown.

## 6.3 Optimal Conditions for NPs Optical Heating

In order to provide deep understanding of the origin of strong heating of low-loss dielectrics, we consider the case of resonant heating, when an external wave is coupled with

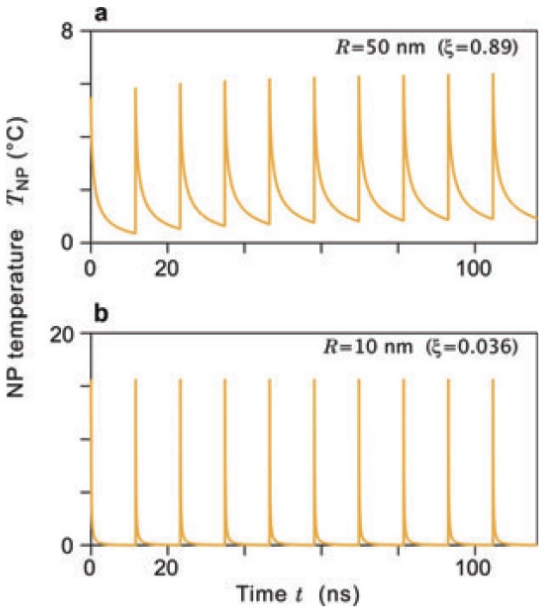


Figure 6.2: Temporal evolution of the temperature of a spherical gold NP of radius $R$ illuminated by a train of pulses with a repetition rate $f$ =86MHz and average irradiance $I = 1mW/m^2$: a) R=50 nm; b) R=10 nm.

an eigenmode of the nanoparticle. The general expression for the absorbed electromagnetic power $Q$ is:

$$Q = \frac{1}{2}\,\mathrm{Re}\int_V \mathbf{J}^\star(\mathbf{r})\cdot\mathbf{E}(\mathbf{r})\mathrm{d}^3r \tag{6.25}$$

where $\mathbf{J}(\mathbf{r})$ is the current density, $\mathbf{E}(\mathbf{r})$ is the electric field inside the material, and the integration is taken over the volume of the nanoobject V. From this formula, it follows that the stronger the electrical field inside the material, the higher the absorbed power. The heating itself is caused by the Ohmic losses determined by the electric conductivity $\sigma$, yielding $J = \sigma E$. Imaginary part of the permittivity determines the conductivity as $\sigma = \epsilon_0\omega Im(\epsilon)$, where $\epsilon_0$ and $\omega$ are the dielectric permittivity of vacuum and incident light frequency, respectively.

Integration in Eq.6.3 over an arbitrary nanoparticle volume supporting eigenmodes allows to rewrite Eq.6.3 in terms of an effective mode volume $V_{eff}$ and spatially averaged field enhancement factor $F = \langle|E|^2\rangle / |E_0|^2$, which determines how much energy can be accumulated inside the nanoparticle and where $|E_0|$ is the incident electric field magnitude. Thus, we can rewrite Eq.6.3 for the absorbed power as:

$$P \sim \sigma F^2 V_{\mathrm{eff}} \tag{6.26}$$

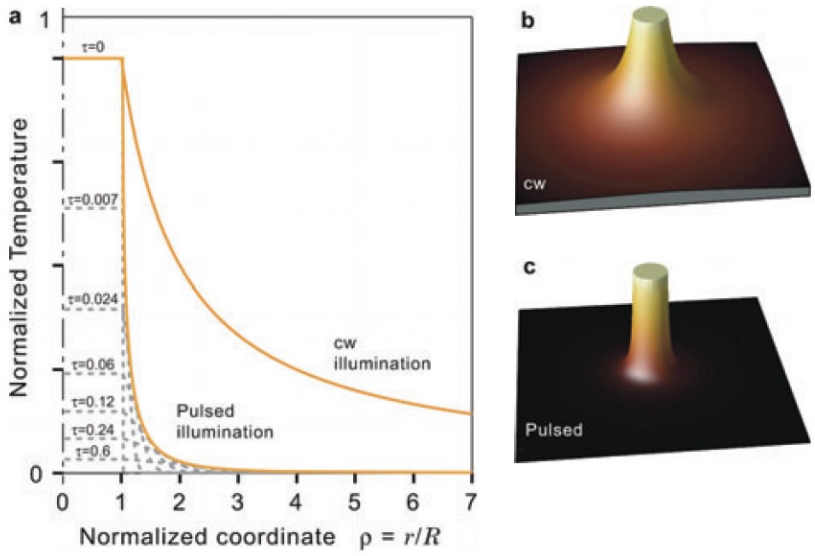


Figure 6.3: Figure comparing the spatial extension of the temperature profile in CW and pulsed illuminations. a) Radial profiles of temperature in both cases. In the case of pulsed illumination, temperature profiles at different normalized time $\tau = t/\tau_{tr}$ are represented (dashed lines) along with the associated temperature envelope. b) Three-dimensional representation of the temperature profile around a NP under CW illumination. c) Three-dimensional representation of the temperature envelope around a NP subsequent to a single femtosecond-pulse illumination

From Eq.6.3 , it is clear that the increasing Ohmic losses do not necessarily lead to the rise of the light absorption by the nanoparticle. On one hand, the imaginary part of the permittivity increases the conductivity but on the other hand it suppresses the quality factor $Q$ of the optical resonance; therefore, the factor $\sigma F^2$ should be considered in more detail.

The field enhancement factor near the nanoparticle resonance $\omega_0$ can be expressed as $F \sim 1/\left(\omega_0^2 - \omega^2 - i\omega\gamma\right)$, where  defines the total optical losses. The optical losses include both radiative and nonradiative (or Ohmic) losses $\gamma = \gamma_{rad} + \gamma_{Ohmic}$. The latter one is proportional to $Im(\epsilon)$, hence the factor $\sigma F^2$ at the resonant frequency $\omega_0$ is proportional to $\sigma F^2 \sim \gamma_{Ohmic}/(\gamma_{rad} + \gamma_{Ohmic})^2$, from which it is clear that for high Ohmic losses the absorbed power tends to zero. Thus, at fixed $\gamma_{rad}$ the maximal value of this factor $\left(\sigma F^2\right)_{\max} \sim 1/\left(4\gamma_{\mathrm{rad}}\right)$ can be achieved when $\gamma_{rad} = \gamma_{Ohmic}$. The radiative losses can be suppressed by considering resonant nanoparticle much smaller than the wavelength $\lambda$, which is the case of small plasmonic nanoparticles, where $\gamma_{\mathrm{rad}} \ll \gamma_{\mathrm{Ohmic}}$. At the surface plasmon resonance $\omega = \omega_0$, the radiative losses are equal to $\gamma_{\mathrm{rad}} \approx \omega_0^3/\omega_{\mathrm{p}}^2(\pi D/\lambda)^3$, where $\omega_p$ is the plasma frequency. This estimation formula gives small values for rad compared to $\omega_0$ due to the ratio $(D/\lambda)^3$. As shown in Fig.6.4a, for small nanoparticles the resonance occurs only in the region of negative $Re(\epsilon)$, and maximal temperature should be achieved at relatively small values of $Im(\epsilon)$, where $\gamma_{rad} = \gamma_{Ohmic}$. On the other hand, for bigger

nanoparticles, which is the case of dielectric ones, the radiative losses for low order dipole modes are high and maximal heating is achieved at higher Ohmic losses (see Fig.6.4b,c). However, for higher order resonances, for example, quadrupole, one can expect small radiative losses and, thus, the maximal optimal heating for lower Ohmic losses that is seen for higher $Re(\epsilon)$ in Fig.6.4b,c.

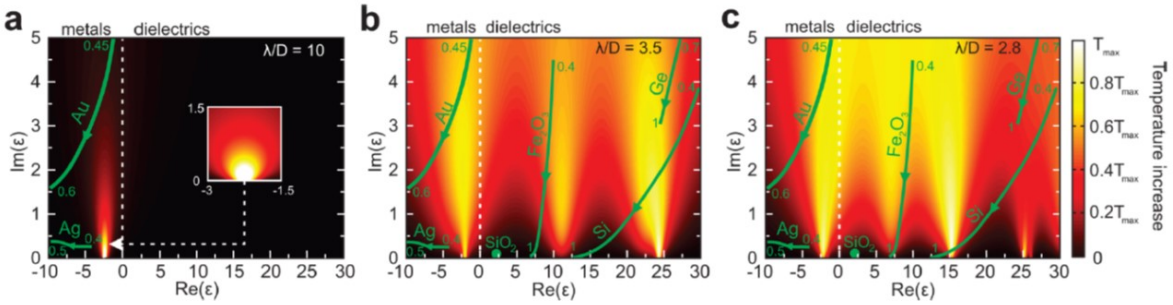


Figure 6.4: Resonant heating of a spherical nanoparticle. Theoretically calculated (Mie theory) heating maps for spherical nanoparticles with fixed wavelength ($\lambda$)/diameter ($D$) ratios for different real and imaginary parts of permittivity in homogeneous medium (air): (a) $\lambda/D = 10$; (b) $\lambda/D = 3.5$; (c) $\lambda/D = 2.8$. Green lines with arrows depict values of $Re(\epsilon)$ and $Im(\epsilon)$ for different materials (dispersion). The orientation of arrows corresponds to increase of wavelength from minimum to maximum indicated by numbers in microns.

Another factor, which is important for the absorption of light, is the effective mode volume inside the nanoparticle $V_{eff}$. Generally, the larger the volume of an arbitrary nanoparticle, the stronger the heating. However, the effective mode volume can significantly affect this dependence. For plasmonic nanoparticles ($Re(\epsilon)$ ¡ 0), the effective volume is defined by a skin depth, which is less than $\delta \approx 20$ nm for most of metals in the visible range. Thus the effective mode volume of plasmonic nanoparticles is $V_{eff} \approx \pi D^2 \delta$. Opposite to metals, dielectrics support optical penetration depth much larger than the diameter of the nanoparticle in the visible range. The effective volumes of Mie-type modes are typically of the order of nanoparticle volume $V_{eff} \approx \pi D^3/6$. It means that the increase of the nanoparticle size is effective for the temperature increase in the case of dielectrics and less effective for the plasmonic nanoparticles.

# Referenses

1. Koroteev N. I., Shumai I. L. Physics of intense laser radiation. - 1991.

2. Baffou G. Thermoplasmonics. - Cambridge University Press, 2017. - P. 101-142.

3. Baffou G., Quidant R. Thermoplasmonics: using metallic nanostructures as nanosources of heat //Laser & Photonics Reviews. - 2013. - V. 7. - . 2. - P. 171-187.

4. Zograf G. P. et al. Resonant nonplasmonic nanoparticles for efficient temperature-feedback optical heating //Nano letters. - 2017. - V. 17. - . 5. - P. 2945-2952.

# Chapter 7

## 7.1 Dec 2013

Q5

a) Apply SOV $u(x,y) = X(x)Y(y)$ gives two ODEs

$$X'' + \lambda X = 0 \tag{7.1}$$

$$Y'' - \lambda Y = 0 \tag{7.2}$$

The Sturm-Liouville associated eqn (7.1) and BC then

$$X'' + \lambda X = 0, \ , X(0) = 0, X(\pi) = 0 \tag{7.3}$$

The solutions are

$$X(x) = c_1 + c_2 x \leftarrow \boxed{\lambda = 0} \tag{7.4}$$

$$X(x) = c_3 \cosh \alpha x + c_4 \sinh \alpha x \leftarrow \boxed{\lambda = -\alpha^2 < 0} \tag{7.5}$$

$$X(x) = c_5 \cos \alpha x + c_6 \sin \alpha x \leftarrow \boxed{\lambda = \alpha^2 > 0} \tag{7.6}$$

$$X(0) = 0 = c_1 + C_2(0) \rightarrow c_1$$
$$X(x) = c_2 x$$
$$X(\pi) = 0 = c_2(\pi) \rightarrow c_2 = 0$$

Thus The solution is trivial. Similarly for eqn (7.5). For eqn (7.6)

$$X(0) = 0 = c_5 (1) + c_6(0) \rightarrow c_5 = 0 \tag{7.7}$$

$$X(x) = c_6 \sin \alpha x \tag{7.8}$$

$$X(\pi) = c_6 \sin \alpha \pi \tag{7.9}$$

For non trivial solution $C_6 \neq 0$ but $\sin \alpha\pi = 0$ that is $\alpha\pi = n\pi \rightarrow \alpha = n$. Thus the solution is

$$X(x) = c_6 \sin nx \tag{7.10}$$

From ODE (7.2) with BC $u(x, 1) = 0 \rightarrow Y(1) = 0$